Protist, Vol. 170, 287–313, July 2019
http://www.elsevier.de/protis
Published online date 9 May 2019

Protist

ORIGINAL PAPER

Acidocalcisomes: Ultrastructure, Biogenesis, and Distribution in Microbial Eukaryotes

Ursula Goodenough[a,1], Aaron A. Heiss[b], Robyn Roth[c], Jannette Rusch[a], and Jae-Hyeok Lee[d]

[a]Department of Biology, Washington University, St. Louis, MO, USA
[b]Division of Invertebrate Zoology and Sackler Institute for Comparative Genomics, American Museum of Natural History, New York, NY, USA
[c]Center for Cellular Imaging, Washington University School of Medicine, St. Louis, MO, USA
[d]Department of Botany, University of British Columbia, Vancouver, Canada

Submitted January 18, 2019; Accepted May 1, 2019
Monitoring Editor: George B. Witman

Acidocalcisomes are membrane-enclosed organelles with acidic lumens that accumulate polyphosphate, often in granular form, and sequester calcium and metals. They carry a transmembrane polyphosphate polymerase and two classes of proton pumps: H^+-pyrophosphatases (H^+-PPases) and V-type ATPases. This report describes acidocalcisomes that were snap-frozen in living cells, primarily the green alga *Chlamydomonas reinhardtii*, and then fractured and etched (QFDEEM). Polyphosphate granules prove to be uncommon in log-phase *C. reinhardtii* cells and abundant in stressed cells, where they are also found within autophagy-related vacuoles. Their E (ectoplasmic) fracture face adopts a unique rugose morphology with etching, and displays ~14 nm globular domains in broken cell preparations. Using etched membrane morphology as a guide, acidocalcisomes were identified during assembly in the trans-Golgi and were recognized in QFDEEM replicas of 18 additional algae and protists. Phylogenetic analysis documents that the eukaryotic gene encoding the signature acidocalcisomal H^+-PPase pump has homologues in three widespread eukaryotic clades and has been lost in opisthokonts and Amoebozoa. The eukaryotic clades are related to three functionally diverged prokaryotic PPase pumps, one of which transports Na^+. Our data indicate that the Last Eukaryotic Common Ancestor (LECA) encoded two bacteria-derived pumps and one Asgard-archaea-derived pump.

© 2019 Elsevier GmbH. All rights reserved.

Key words: Acidocalcisomes; polyphosphate granules; *Chlamydomonas reinhardtii*; freeze-fracture; phylogenetic analyses; Asgard archaea.

Introduction

Polyphosphate is a polymer of three to hundreds of phosphoanhydride (P ~ P) units (equivalent to the ADP ~ P bond in ATP) that is found in all present-

[1]Corresponding author.
e-mail goodenough@wustl.edu (U. Goodenough).

https://doi.org/10.1016/j.protis.2019.05.001
1434-4610/© 2019 Elsevier GmbH. All rights reserved.

day organisms (Achbergerova and Nahalka 2011; Kornberg et al. 1999; Moreno and Docampo 2013; Rao et al. 2009). Pyrophosphate (P ~ P or PPi), when released from the polymer or when generated by anabolic reactions in the cytoplasm, can be hydrolyzed by pyrophosphatases (PPase) to perform work; exo- and endopolyphosphatases also catalyze the release of orthophosphate (Pi) from polyphosphate polymers.

Phosphate homeostasis in algae, fungi, and protists is closely intertwined with regulation of polyphosphate levels (Wild et al. 2016; reviewed in Azevedo and Saiardi 2017). Much of the phosphate in oceans takes the form of polyphosphate, posited to derive from marine organisms (Diaz et al. 2008), although it may also have formed pre-biotically (Rao et al. 2009), and plankton accumulates and cycles polyphosphate in response to low phosphorous conditions (Martin et al. 2014). Polyphosphate polymerization is catalyzed by a polyphosphate kinase (PPK) in bacteria and in some unicellular eukaryotes (Blaby-Haas and Merchant 2017; Brown and Kornberg 2004; Hooley et al. 2008), and by polyphosphate-polymerase activity associated with the vacuolar transporter chaperone (VTC) complex in yeast (Desfougères et al. 2016; Hothorn et al. 2009; Martinez et al. 2015) and in protists and algae (Askoy et al. 2014; Blaby-Haas and Merchant 2017; Fang et al. 2007; Ulrich et al. 2014) but not yet identified in animals or land plants.

A widespread consumer of PPi is a pyrophosphate-activated proton pump (H^+-PPase) (Au et al. 2006; Drozdowicz et al. 2003; Hsu et al. 2009; Kim et al. 1994; McIntosh and Vaidya 2002; Rea et al. 1992; Rodrigues et al. 1999; Schilling et al. 2017; Segami et al. 2017; Serrano et al. 2007; Shah et al. 2017; reviewed in Tsai et al. 2014). The pump participates in acidifying the lumens of land-plant vacuoles (Asaoka et al. 2014; Tommi et al. 2013; Venter et al. 2006) and of organelles called acidocalcisomes.

Acidocalcisomes (Vercesi et al. 1994) were originally recognized because they harbor an internal polyphosphate granule (Docampo and Huang 2016; Docampo 2016; reviewed in Miranda et al. 2008). They were then found to acidify their lumens to pH 5-5.5 using both the ubiquitous V-type ATPase and the H^+-PPase proton pump (Scott and Docampo 2000), and to accumulate calcium, potassium, and various cationic metals and organic molecules via acid-dependent transporters/exchangers (Hong-Hermesdorf et al. 2014; Kaska et al. 1985; Klompmaker et al. 2017; Komine et al. 2000; Penen et al. 2016, 2017; Ruiz et al. 2001a, b; Siderius et al. 1996; Steinmann et al. 2017; Vercesi et al. 1994).

The proteomes of acidocalcisomes isolated from the red alga *Cyanidioschyzon merolae* and kinetoplastids (Huang et al. 2014; Lee et al. 2007; Yagisawa et al. 2009) also feature hydrolytic enzymes and components of vesicular trafficking pathways such as Rabs and SNAREs that are involved in their biogenesis (Besteiro et al. 2008; Huang et al. 2011; Li and He 2014; Niyogi et al. 2015); aquaporins have also been identified (Montalvetti et al. 2004). Recently, soluble inositol pyrophosphates, which regulate many cellular activities (reviewed in Cordeiro et al. 2017), and an acidocalcisome-localized IP_3 receptor (Huang et al. 2013; Lander et al. 2016) have been shown to participate in Ca^{2+} homeostasis (reviewed in Ramakrishnan and Docampo 2018).

Acidocalcisomes have been implicated as important or essential to the disease cycles of trypanosomatid and apicomplexan parasites (Da Silva and Beverly 2010; de Jesus et al. 2010; Fang et al. 2007; Kohl et al. 2018; Li and He 2014; Luo et al. 2005; Moreno and Docampo 2009; Ruiz et al. 2004a) and as possible drug targets (Docampo and Moreno 2008; Pinto-Martinez et al. 2018). Until recently they were thought to be restricted to algae and protists, but acidic "lysosome-related organelles" with similar properties (polyphosphate and calcium storage but lacking the H^+-PPase pump) have been reported in some animal cell types (Huizing et al. 2008; Ruiz et al. 2004b; Moreno-Sanchez et al. 2012; Muller et al. 2009; reviewed in Morrissey et al. 2012), and the yeast vacuole has been referred to as acidocalcisome-like (Gerasimaitè and Mayer 2017) even though it too lacks the H^+-PPase.

Unlike most ubiquitous eukaryotic organelles, acidocalcisome ultrastructure is poorly described because it is poorly preserved using fixation/dehydration protocols (Docampo et al. 2005). Reported here is a detailed ultrastructural analysis of the acidocalcisome, largely in the eukaryotic green alga *Chlamydomonas reinhardtii* but also in 18 additional algae and protists, using living cells snap-frozen at liquid helium temperatures, subjected to freeze-fracture, deep-etching (surface water sublimation under vacuum), and platinum rotary-replication, and viewed by transmission EM (QFDEEM) (Heuser 2011).

We document that acidocalcisomes display a unique membrane ultrastructure when viewed by QFDEEM. The concave half-membrane contigu-

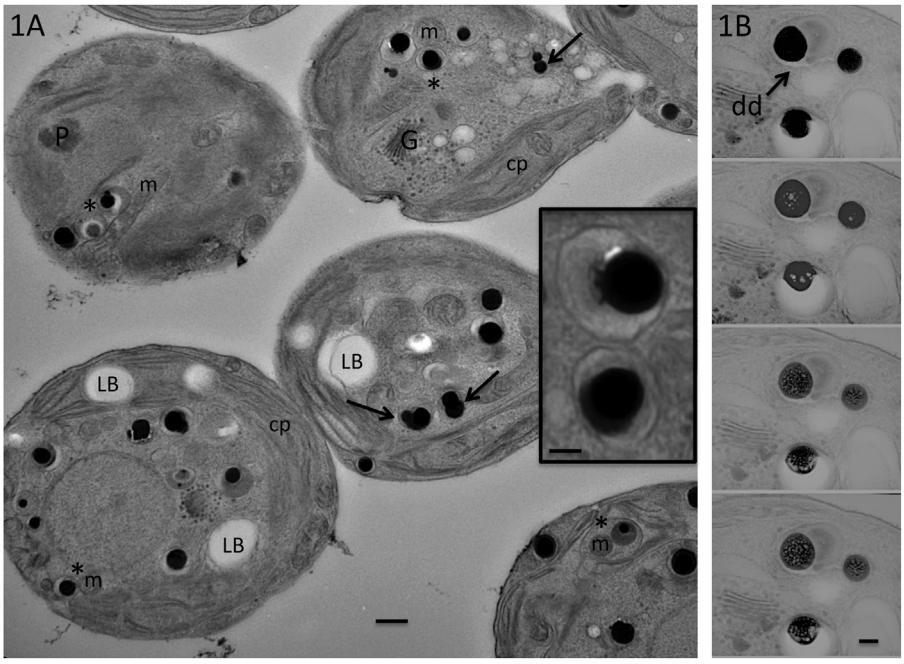

Figure 1. Acidocalcisome thin sections. Freeze-substituted *sta6* cells 30 h N-starve from stationary phase. (**A**) Cell survey. Polyphosphate granules are black. LB, lipid body; P, pyrenoid; cp, chloroplast; m, mitochondrion; G, Golgi. Arrows: two granules likely enclosed in a vacuole; asterisks: close association of acidocalcisomes and mitochondria. Bar, 500 nm. Inset: Two "twin" acidocalcisomes showing the amorphous material in their lumens. Bar, 200 nm. (**B**). Three acidocalcisomes left under electron beam in the TEM for several minutes, causing the granules to "fry" and bubble. The inclusion in the double decker (dd) acidocalcisome is not affected. Bar, 200 nm.

ous to the cytoplasm (the P fracture face) carries a dense population of small intramembranous particles (IMPs), while the convex half-membrane contiguous to the lumen (the E fracture face) is smooth in the absence of etching and becomes distinctively rugose when exposed to etching. The E-face rugosities differentiate into clusters of ~14-nm globular profiles in broken/fractionated preparations of *C. reinhardtii* cells. This distinctive freeze-fracture membrane morphology has permitted identification of acidocalcisomes being assembled in the trans-Golgi and in a wide variety of algae and protists. We also report that in *C. reinhardtii*, polyphosphate granules are largely restricted to the acidocalcisomes of stressed cells, where they also become included in autophagy-related vacuoles.

Finally, we expand previous phylogenetic analyses of the signature H^+-PPase pump (Kellosalo et al. 2007; Luoto et al. 2011; Medeiros et al. 2011; Perez-Castineira et al. 2002; Seufferheld et al. 2011). We document three widespread eukaryotic PPase clades, two of which have apparently derived from bacteria and one from archaea.

Results

Frozen Thin-sectioned Acidocalcisomes

Figure 1A shows thin sections of *C. reinhardtii sta6* cells, starved for nitrogen (N) for 30 h from stationary phase, that were snap-frozen and freeze-substituted with OsO_4. The sections are sufficiently thick to retain the electron-dense polyphosphate granules that otherwise tend to fall out due to incomplete plastic infiltration (Armbrust et al. 1995; Da Silva and Beverly 2010; Docampo et al. 2005; Kaneko et al. 2007). Figure 1B shows, as previously observed (Ruiz et al. 2001a), that these granules vaporize with exposure to the electron beam, as do the contents of lysosome-related organelles (Ruiz et al. 2004b).

As detailed in later sections, granules are prominent in the acidocalcisomes of *C. reinhardtii* cells that have entered stationary phase and/or are subjected to stresses such as N-withdrawal. They are also found within vacuoles in stationary/stressed cells. Distinguishing acidocalcisomes from vacuoles, while straightforward in QFDEEM replicas using membrane fracture-face morphology as a

guide, is difficult in thin sections, but since multiple granules have never been observed in fractured acidocalcisomes but are often observed in fractured vacuoles, the double-granuled organelles denoted with arrows in Figure 1A are likely to be vacuoles.

Acidocalcisomes are occasionally contiguous to one another (Fig. 1A inset), a configuration we designate as "twins," and are often contiguous to other organelles as well, most commonly mitochondria (Fig. 1A, asterisks; Supplementary Material Fig. S1A), as has also been noted in *Trypanosoma brucei* (Ramakrishnan et al. 2018).

Cross-fractured Acidocalcisomes: Granules and Other Internal Content

Figure 2 and Supplementary Material Figure S1D show acidocalcisomes from snap-frozen un-fixed *C. reinhardtii* cells that were cross-fractured, deep-etched, and Pt-replicated to reveal their granules (g) and internal content (i). The granules, ranging in size from 200–600 nm, are either smooth (Fig. 2A, E, G-I), pockmarked (Fig. 2B, F) or layered (Fig. 2C-D), where the irregularities may be native or generated during the fracturing process. The internal content consists of heterogeneous material that is similar in texture to the proteinaceous interiors of other organelles such as the mitochondrial matrix. Cross-fractured acidocalcisomes are uncommon: the fracture plane usually travels within the plane of the acidocalcisome membrane and around any internal granule.

Cross-fractured Acidocalcisomes: "Double-decker" Variants

Figure 3 and Supplementary Material Figure S1C show acidocalcisomes that we call "double deckers," possessing both a polyphosphate granule and a second round, fluffy inclusion (fi). Figure 1B includes such a variant (dd) in thin section; notably, the inclusion does not froth with electron-beam exposure like the polyphosphate granule, indicating that it is not composed of inorganic salt. Internal membrane profiles (im) are commonly included within double deckers. Double deckers are far less frequently encountered than granule-only acidocalcisomes.

Acidocalcisome Membrane Interior: P-face

Figure 4A-C shows "twin" acidocalcisomes (cf Fig. 1A inset) where the fracture plane has exposed the P-face (the half-membrane contiguous to the cytoplasm) of the upper organelle and the E-face (the half-membrane contiguous to the lumen) of the lower organelle, illustrating their very different ultrastructure. Figure 4D illustrates that at least in some cases, the twins may be interconnected by a shared membrane bridge.

Figures 5 and 6 and Supplementary Material Figures S1B and S2 present additional micrographs of acidocalcisomal P-faces (see also Robinson et al. (1998), figs 6 and 7). When fractures follow the deep concave configuration of the membrane (Fig. 5A; Supplementary Material Figs. S1B and S2), intramembranous particles (IMPs) are poorly highlighted by rotary-shadowing. More planar views (Fig. 5B) reveal numerous small IMPs, presumably representing trans-membrane protein domains (Severs 2007).

The P fracture faces in Figures 4, 5A and B and Supplementary Material Figures S1B and S2 were subjected to deep-etching, which generates irregular "pits" (arrows) that are created when an IMP is pulled into the opposite E-face during fracture, leaving a hole that enlarges with water sublimation. Such pits are absent when the P-face is not etched (Figs 5C, 6B and D) or lightly etched (Figs 5D, 6A and C). The IMPs range in density from tightly packed (Figs 4B, 5B, C, 6C-D) to more dispersed (Figs 4A, C, 5D, 6A), and they may line up in linear or curved arrays (Figs 4C, 5C-D).

Acidocalcisome Membrane Interior: E-face

The ultrastructure of the E-faces of *C. reinhardtii* acidocalcisomes is uniquely sensitive to deep-etching. Figure 6A and C shows lightly-etched E-faces, and Figure 6B and D shows non-etched E-faces. In all cases, the faces are smooth, with a modest endowment of large IMPs. Figure 7A and B shows uncommon examples of deep-etched specimens where a smooth fracture face is retained but transitions into a rugose morphology, and Figures 2, 4, 7C-G, and Supplementary Material Figures S1 and S2 show the fully rugose morphology that is displayed in most deep-etched samples. Figure 8A and B shows a rare example of a smooth E-face transitioning into discrete worm-like domains which, we propose, proceed to collapse into the full rugose configuration. Collectively, these images indicate that the E-face morphology of the acidocalcisome is distinctively sensitive to the etching process.

Deep-etched E-faces often also display a flattened rim (R) around the periphery (Fig. 7C-G) which is not observed in non-etched profiles. Rims are also occasionally observed in deep-etched concave P-face profiles (Fig. 5A). Possibly

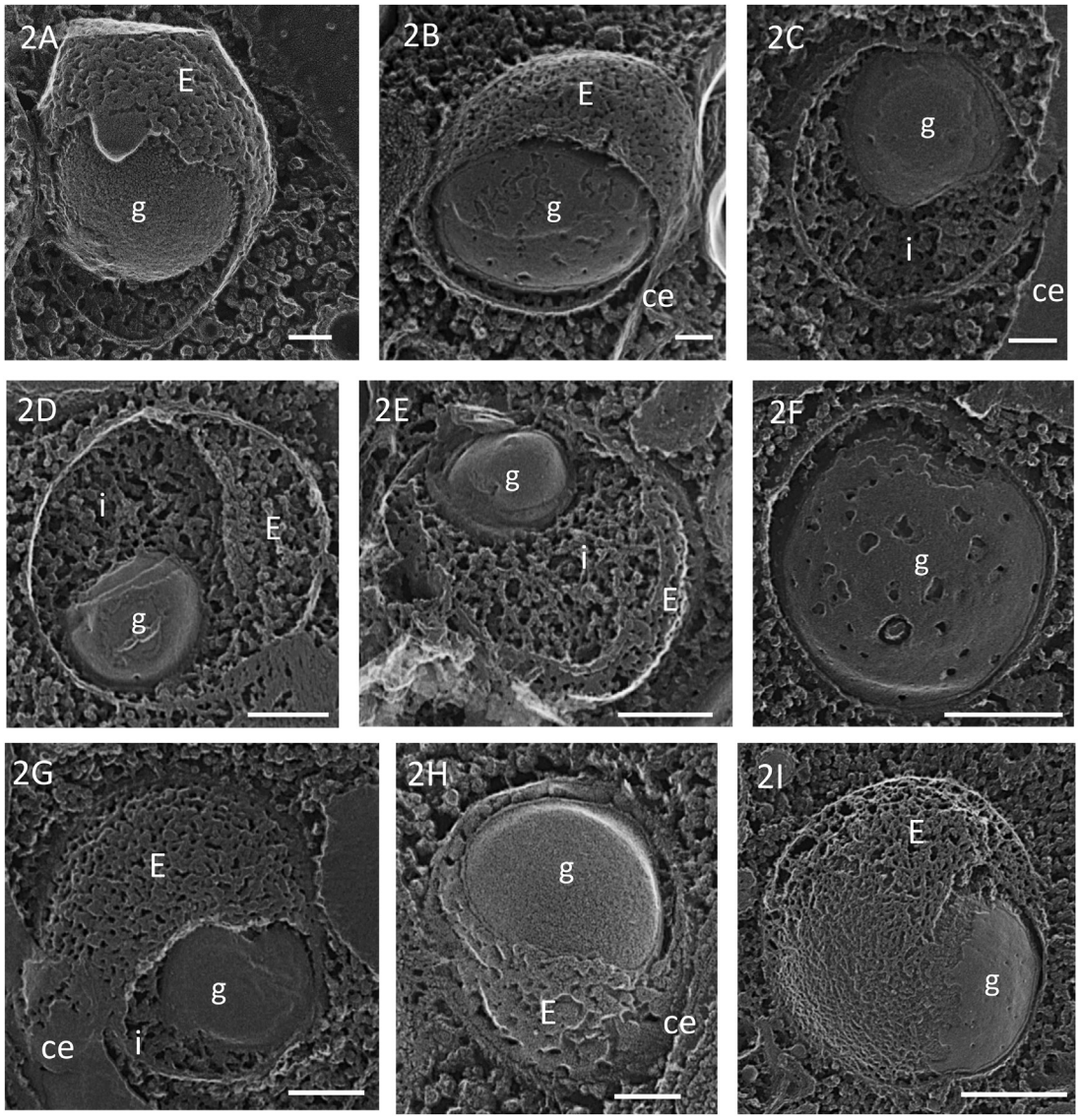

Figure 2. Cross-fractured acidocalcisomes. g, polyphosphate granule; i, internal lumen content; E, E-fracture face of acidocalcisome membrane; ce, chloroplast envelope. (**A**) *cw15* 48 h N-starve from log phase. Bar, 100 nm. (**B**) *sta6* 30 h N-starve from stationary phase. Bar, 100 nm. (**C**) *sta6* 12 h N-starve from stationary phase. Bar, 100 nm. (**D**) *sta6* 12 h N-starve from stationary phase. Bar, 200 nm (**E**) *sta6* 12 h N-starve from stationary phase. Bar, 200 nm (**F**) *sta6* 48 h N-starve from log phase no acetate. Bar, 500 nm. (**G**) *sta6* 12 h N-starve from stationary phase. Bar, 200 nm. (**H**) Wild-type stationary phase (7-day agar plate). Bar, 100 nm. (**I**) *sta6* 8 h N-starve from log phase. Bar, 500 nm.

this structure represents the etched cytoplasmic domains of the pumps and transporters that associate with acidocalcisomes.

Globular Domains in the Acidocalcisome E-face

Figure 8C and D show the sole example encountered in this study where the smooth E-face of a native acidocalcisome displays distinctive globular domains, with central depressions, that are ~17 nm in diameter, or ~14 nm in diameter after subtracting the 3 nm of platinum added during rotary replication. This image derives from a QFDEEM sample of the colonial green alga *Botryococcus braunii* (Weiss et al. 2012); comparable domains have not been recognized in native *C. reinhardtii* acidocalcisomes.

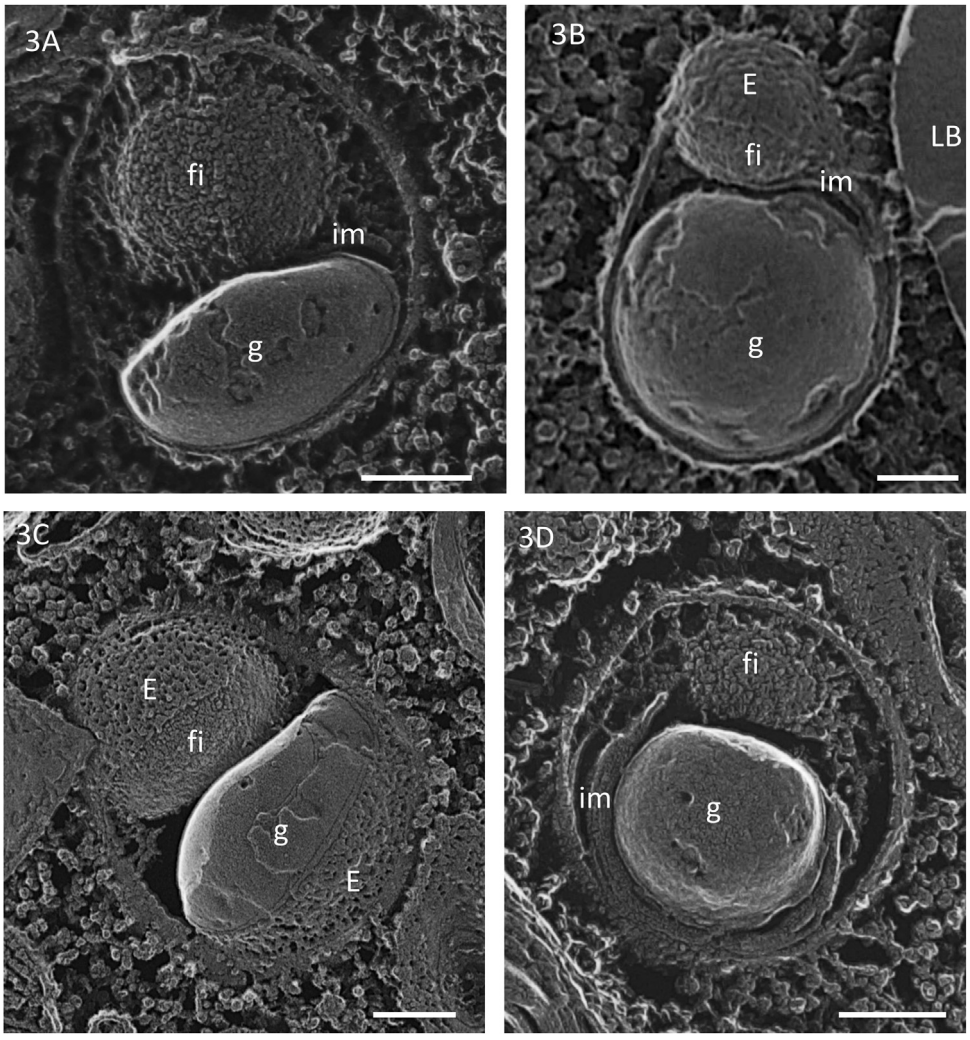

Figure 3. Double deckers. Cross-fractured double-decker variant of the acidocalcisome showing polyphosphate granules (g) and fluffy inclusions (fi). E, E-fracture face of acidocalcisome membrane; im, internal membrane; LB, lipid body. (**A**) *sta6* 30 h N-starve from stationary phase. Bar, 100 nm. (**B**) *sta6* 30 h N-starve from stationary phase. Bar, 100 nm. (**C**) Complemented *sta6* 48 h N-starve from log phase. Bar, 200 nm. (**D**) *sta6* 30 h N-starve from stationary phase. Bar, 100 nm.

When, however, log-phase *C. reinhardtii* acidocalcisomes were visualized after cell breakage into a solution containing digitonin and mannitol (see Methods), many E-faces display not only rugose regions but also closely packed arrays of globular domains (Fig. 9), with central depressions, ~17 nm in diameter or ~14 nm when platinum coating is subtracted, that may correspond to those seen in *B. braunii*. In many regions the globular arrays are apparently confluent with the rugose domains, consonant with the hypothesis that they represent two configurations of the same materials. No such globular domains were evident in the E-faces of acidocalcisomes isolated from stationary-phase cells in a second experiment; whether this reflects technical variation or a difference in the membranes under these two growth conditions will require additional experimentation. The membranes of all other organelles in the broken preparations retain their in situ morphology, notably the F-type pump-laden mitochondrial cristae (Supplementary Material Fig. S3).

Acidocalcisome Biogenesis at the trans-Golgi

Figure 10A-E shows acidocalcisomes being assembled at the trans-face of the Golgi in *C. reinhardtii*, where small vesicles occasionally appear to be fusing with the organelle mem-

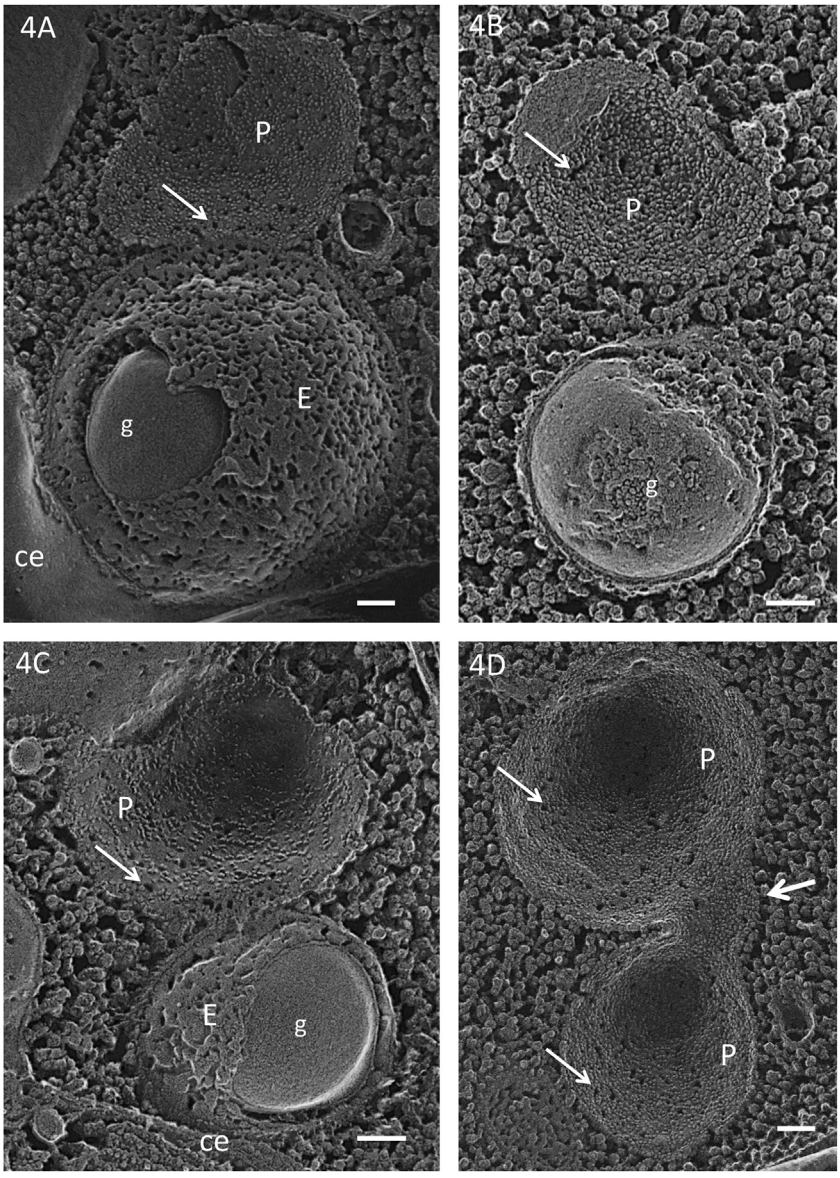

Figure 4. "Twin" acidocalcisomes. P, P-fracture face; E, E-fracture face; g, polyphosphate granule; ce, chloroplast envelope; small arrows, P-face pits. Bars, 100 nm. (**A**) Wild-type 24 h N-starve from log phase. (**B**) *cw15* log phase. (**C**) *cw-15* stationary phase (7-day agar plate). (**D**) Two acidocalcisome P-faces connected by a bridge (large arrow).

brane (Fig. 10D and E, asterisks). Comparable images have been obtained in *Chlamydomonas monoica* (Fig. 10F) and the trypanosomatid *T. brucei* (Fig. 10G). Acidocalcisomes associated with the Golgi are smaller than most of those localized elsewhere in the cytoplasm; nothing is known about how they increase in size. One cross-fractured Golgi-associated acidocalcisome reveals an internal granule (Fig. 10E), indicating that granule and organelle biogenesis can be concurrent.

Granule Formation is Stimulated by Stress Conditions in *C. reinhardtii*

Log-phase *C. reinhardtii* cells produced abundant acidocalcisomes (e.g. Figs 5, 6, 7D-G, 10D-E), as recognized by the ultrastructure of their fractured membranes, but we have found only one example of a polyphosphate granule within the acidocalcisome of a log-phase cell (Fig. 4B). All of our other images of granule-containing acidocalcisomes come from cells that are under stress – they are either entering or in stationary phase or have been subjected

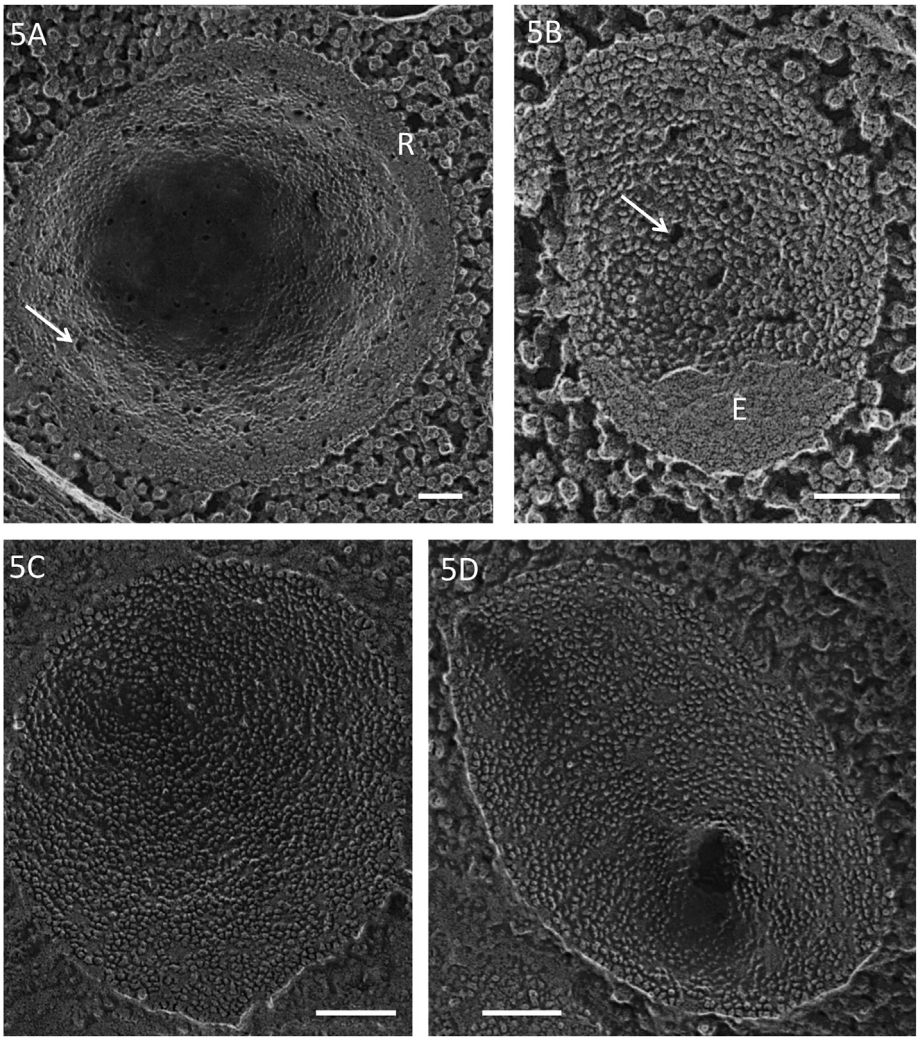

Figure 5. P fracture faces of acidocalcisomes. E, E-fracture face; R, rim; arrows, pits. Bars, 100 nm. (**A**) *sta6* log phase, deep-etch. (**B**) *cw15* log phase, deep-etch. (**C**) *sta6* log phase no-etch. (**D**) *sta6* log phase light-etch.

to N-starvation (Figs 1–4 and 10, Supplementary Material Fig. S1). Hong-Hermesdorf et al. (2014) and Askoy et al. (2014) similarly note that granules are absent from log-phase and present in stressed Zn-deprived and sulfur-deprived cells respectively, and in other EM reports where granules are illustrated, cells were fixed in stationary phase (Komine et al. 2000), "late-log/exponential phase" (Gal et al. 2018; Penen et al. 2016, 2017; Ruiz et al. 2001a) – i.e. entering stationary phase – or N-starved (Siderius et al. 1996).

When *sta6* cells were N-starved for 48 h and then transferred to N-containing media and sampled after 12 or 17 hours, smooth-edged granules were present in the starved sample but absent from the N-supplemented samples, indicating that the granules can be resorbed when stress is alleviated. Candidate images of this process are shown in Supplementary Material Figure S4. Some acidocalcisomes contained granules with irregular edges (Supplementary Material Fig. S4A and B), possibly illustrating the dissolution stage. Others contained homogeneous material (Supplementary Material Fig. S4C-D), possibly corresponding to polyphosphate in a gel configuration (see Discussion); similar homogeneous material, apparently continuous with aggregated internal content, is present in a log-phase non-etched sample (Supplementary Material Fig. S4E). Others contained only aggregated material (Supplementary Material Fig. S4F and G), possibly corresponding to polyphosphates in a sol configuration (see Discussion) that have coalesced during the etching process. In some log-phase acidocalcisomes, a puddle of gel-like

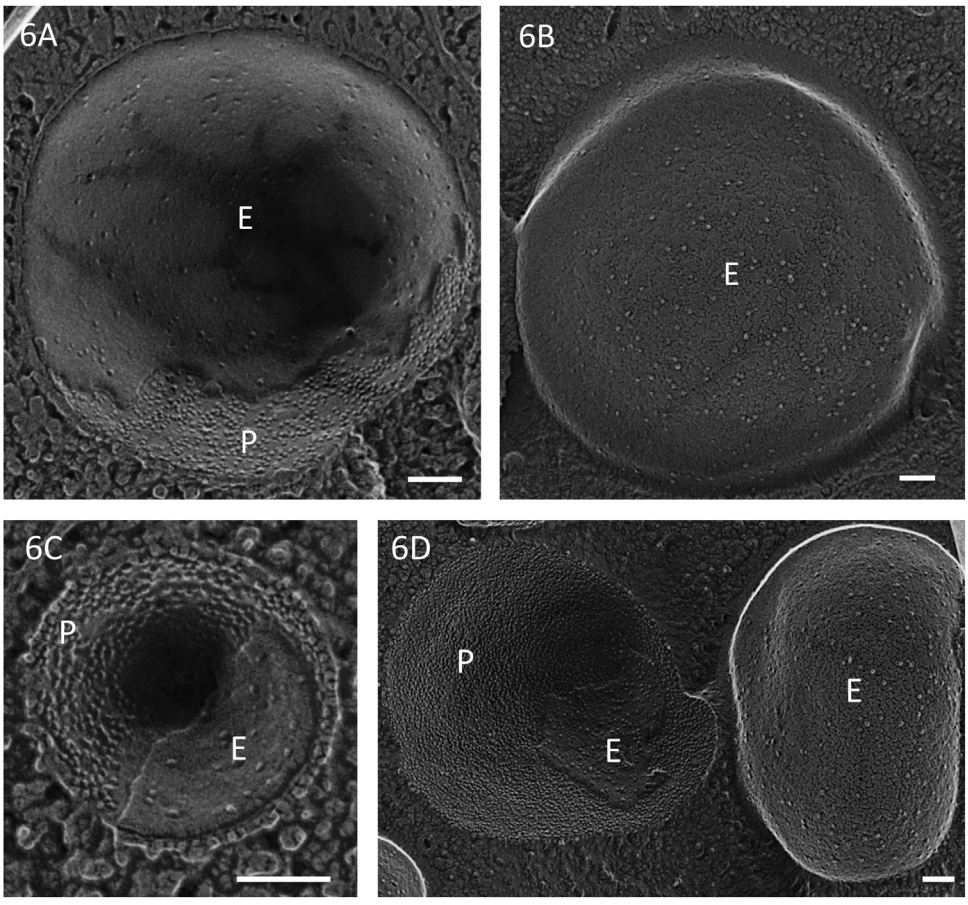

Figure 6. E fracture faces of acidocalcisomes. Light-etch (**A** and **C**) and no-etch (**B** and **D**) acidocalcisomes in *sta6* log phase cells. Figure D shows a "twin." P, P-face. Bars, 100 nm.

material remains in the interior after etching (Supplementary Material Fig. S4H).

In Stressed Cells, Granules are Found Within Both Vacuoles and Acidocalcisomes

The cytoplasmic vacuoles of log-phase *C. reinhardtii* cells are small, usually round, and devoid of granules or membranous material (Fig. 11 and Supplementary Material Fig. S5C). Their P fracture faces (Fig. 11A and C) contain small tightly-packed IMPs resembling acidocalcisome P-faces, but their deep-etched E-faces (Fig. 11B) are flat with numerous irregular pits that are readily distinguished from the rugose E-faces of acidocalcisomes. When cells are grown in phosphate-buffered media the log-phase vacuole contents are finely particulate (Supplementary Material Fig. S5C) or fibrillar (Fig. 11A), whereas when grown in Tris-buffered media they also contain long fibers, of unknown etiology or composition (Fig. 11C and Supplementary Material Fig. S5A and B), which persist in the vacuoles of N-starved (Martin and Goodenough 1975) and stationary-phase (Supplementary Material Fig. S5A and B) cells.

Stressed *C. reinhardtii* cells contain several vacuolar populations, where a full report is in preparation. Relevant here are vacuoles containing polyphosphate granules as well as membrane fragments and other cellular debris, indicating that they are autophagy-related. Figure 12 and Supplementary Material Figure S5D-F show representative images; an example is also provided in Goodenough et al. (2014, fig. 3), where we also document increased expression of autophagy-related genes with N-starvation. Autophagy-related vacuoles are distinguished from acidocalcisomes by four criteria: a flat/pitted rather than a rugose E-face (Fig. 12A and B; Supplementary Material Fig. S5E); the common inclusion of more than one granule (Fig. 12A-D; Supplementary Material Fig. S5F); the common presence of membranous debris (Fig. 12E; Supplementary Material Fig. S5D and

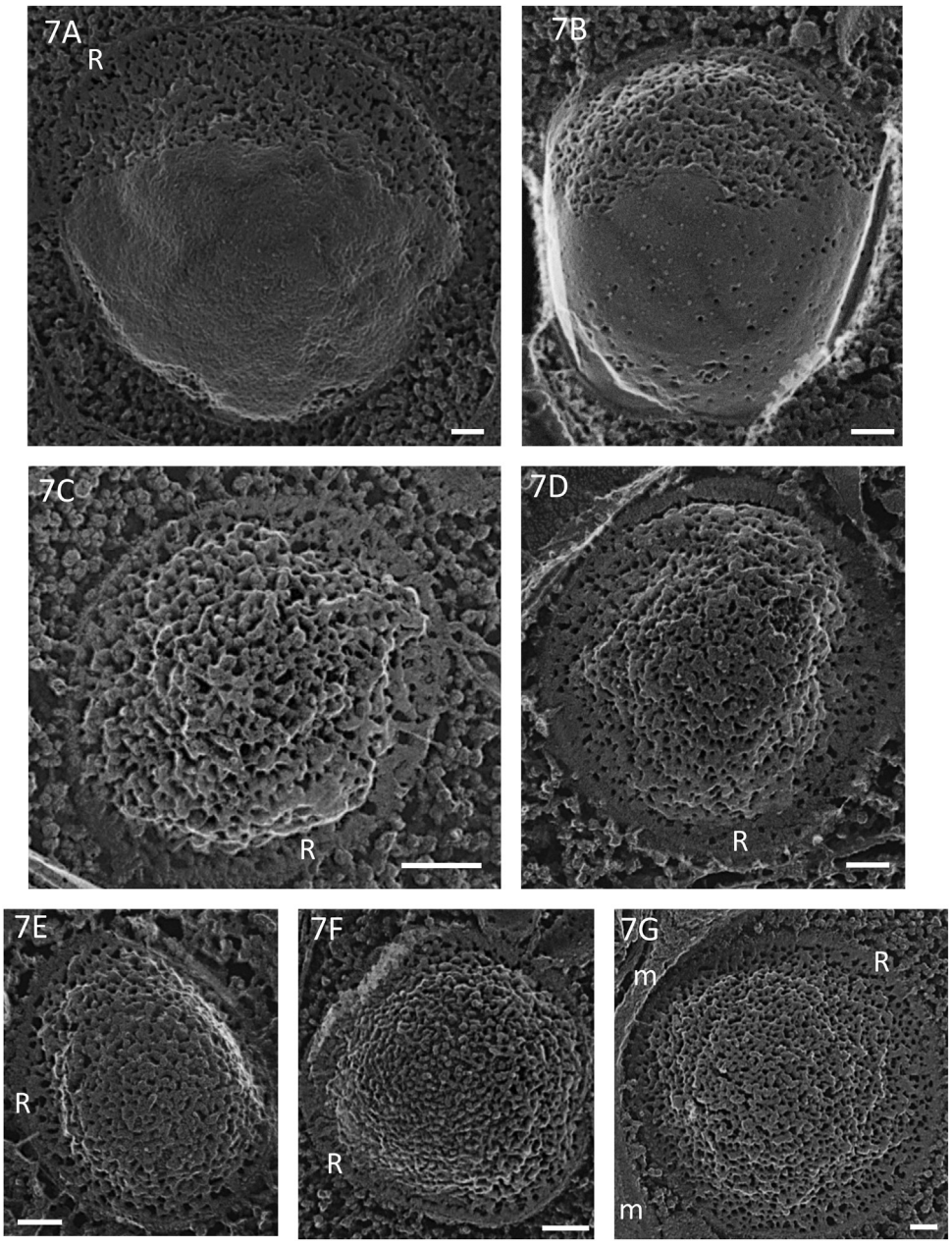

Figure 7. E fracture faces of acidocalcisomes. R, rim; m, mitochondrion. Bars, 100 nm. **A**) *sta6* 2 h N-starve from log phase. (**B**) Complemented *sta6* 48 h N-starve from log phase. (**C**) *sta6* 48 h N-starve from log phase, no acetate. (**D**) *cw15* log phase. (**E**) *sta6* 48 h N-starve, 8 h N-replete. (**F**) *cw15* log phase. (**G**) *sta6* 48 h N-starve, 8 h N-replete.

E; fig. 3 of Goodenough et al. 2014); and usually a much larger and more irregular size and shape. Figure 12D shows a stationary-phase vacuole from a Tris-buffered cell containing both a granule and the long fibers that also mark their log-phase vacuoles, indicating that the same class of vacuole lacks granules during growth and acquires granules with stress.

Expression Levels of Acidocalcisome-related Genes under Stress

Several studies have documented that autophagy-related genes are up-regulated by stress in *C. reinhardtii* (Goodenough et al. 2014; Pérez-Pérez et al. 2012; Ramundo et al. 2014; Schmollinger

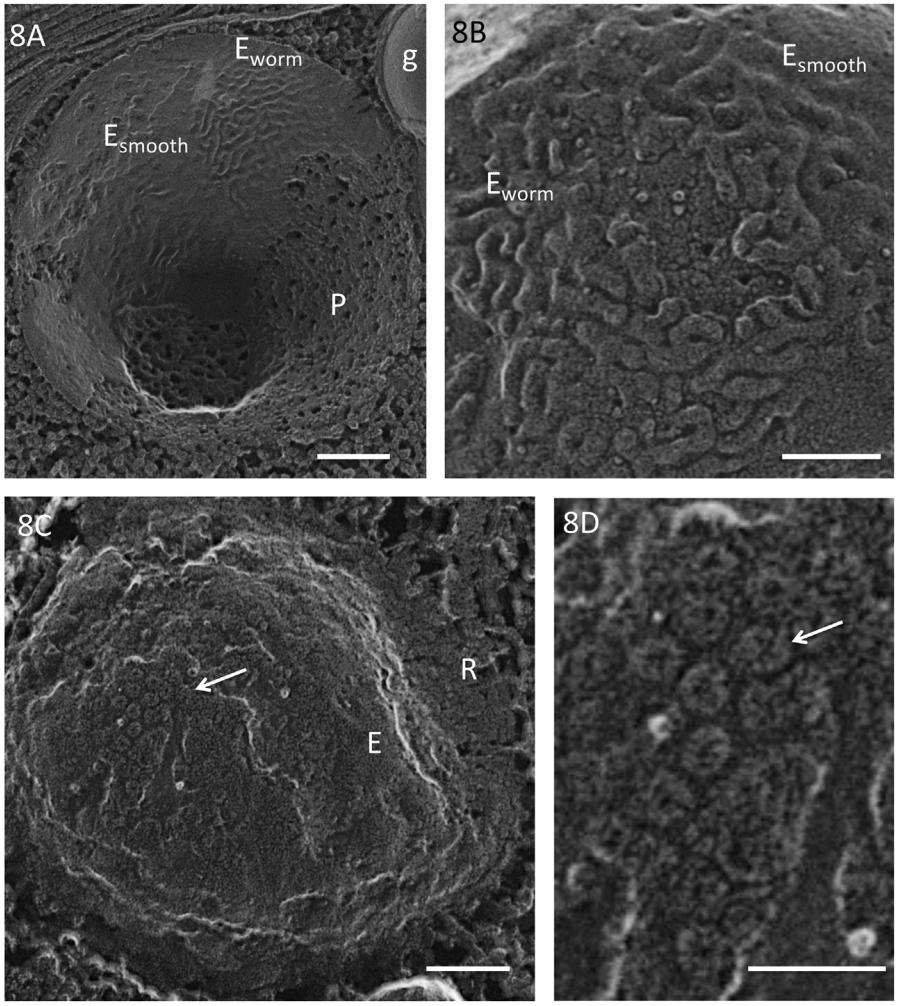

Figure 8. E fracture faces of acidocalcisomes. (**A**) Candidate "worm" stage of transition from smooth to rugose morphology of etched acidocalcisome E-face; P, P face; g, granule in twin acidocalcisome. *cw15* stationary phase. Bar, 200 nm. (**B**) Second example of "worm" configuration. *cw15* stationary phase. Bar, 100 nm. (**C**) Acidocalcisome of *Botryococcus braunii*. E, smooth E-face; R, rim; arrow, globular domains within the E-face. Bar, 100 nm. (**D**) Enlargement of globular domains in (C). Bar, 50 nm.

et al. 2014). To ask whether acidocalcisome-associated genes also follow this pattern, we monitored the expression levels of two genes under two stress conditions: N-starvation and entrance into stationary phase. The results are shown in Supplementary Material Table S1. Levels of *VTC1* expression, a subunit of the VTC complex that also includes the polyphosphate polymerase subunit VTC4, remained relatively stable under both conditions, as Askoy et al. (2014) have also observed in S-starved cells. By contrast, levels of *AVP1* transcripts, encoding the H^+-PPase, decreased 2-4 fold.

Conservation of Acidocalcisome Membrane Morphology in Algae and Protists

Supplementary Material Figures S6-S8 show candidate acidocalcisomes from a variety of unicellular eukaryotes. In each case, the organelles were identified by one or more of the features that characterize the deep-etched acidocalcisomes of *C. reinhardtii*: 1) a concave P-face with a dense population of small IMPs and occasional rims; 2) a convex E-face with a smooth → rugose membrane and frequent rims; and 3) exposure of a

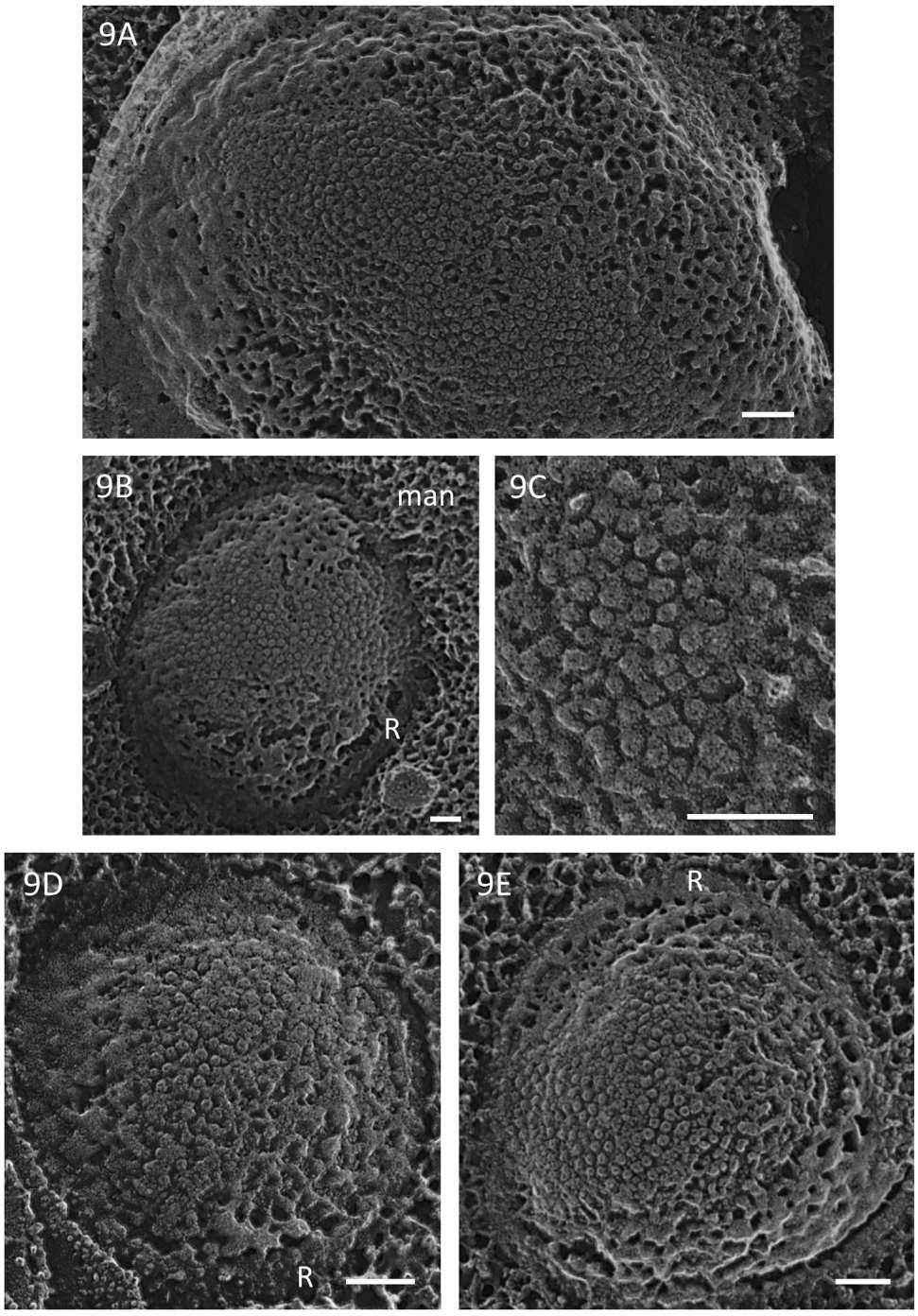

Figure 9. Cell-free acidocalcisomes. *C. reinhardtii sta6* log-phase cells lysed via digitonin/osmotic shock into a mannitol (man) solution, exposing globular domains in the E face. R, rim. Bars, 100 nm.

granule. The 18 species surveyed represent most of the unicellular eukaryotic photosynthetic radiations as well as an apicomplexans (*Neospora caninum*), an "excavate" amoeba (*Naegleria gruberi*), and an "excavate" trypanosomatid (*T. brucei*). As expected, no candidates were identified in the fungi *Saccharomyces cerevisiae* or *Cryptococcus neoformans*. While the P-faces are strikingly similar in all the organisms examined, the etched E-faces are far more variable in morphology, mirroring their variability in *C. reinhardtii*.

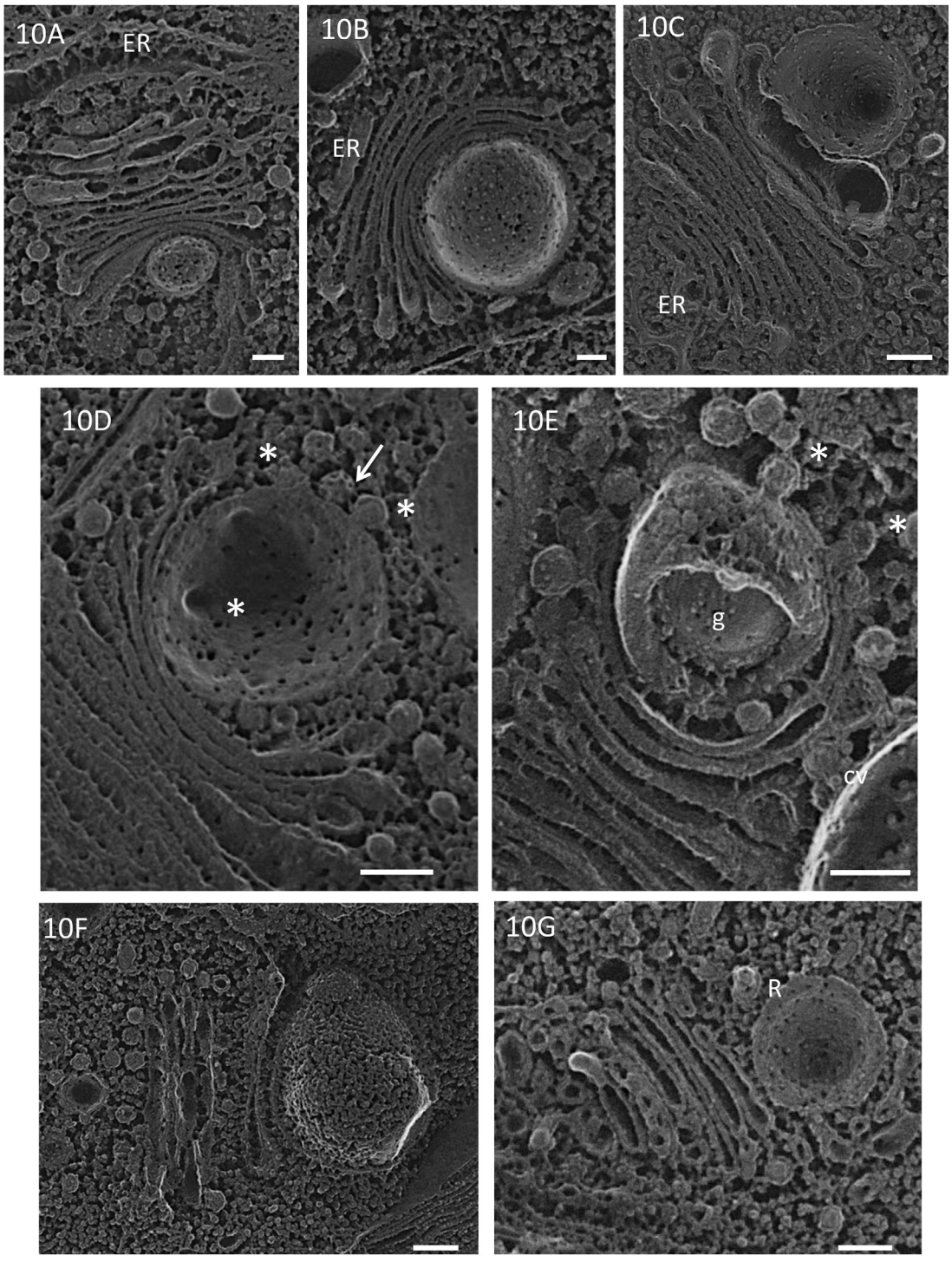

Figure 10. Acidocalcisomes assembling at trans-Golgi face. *C. reinhardtii* (**A-**E), *Chlamydomonas monoica* (**F**) and *Trypanosoma brucei* (**G**). g, polyphosphate granule; R, rim; asterisks, Golgi vesicles fusing with acidocalcisome; arrow, clathrin-coated vesicle. Bars, 100 nm. (**A**) Rugose E-face, *sta6* 48 h N-starve from log phase, 8 h N-replete. (**B**) Smooth E-face, 48 h N-starve, 17 h N-replete. (**C**) P-face, *cw15* 30 h N-starve from log phase. (**D**) P-face, *sta6* log phase light-etch. (**E**) Rugose E-face with granule and fusing golgi vesicles, *cw15* 96 h N-starve. (**F**) Rugose E-face. (**G**) P-face.

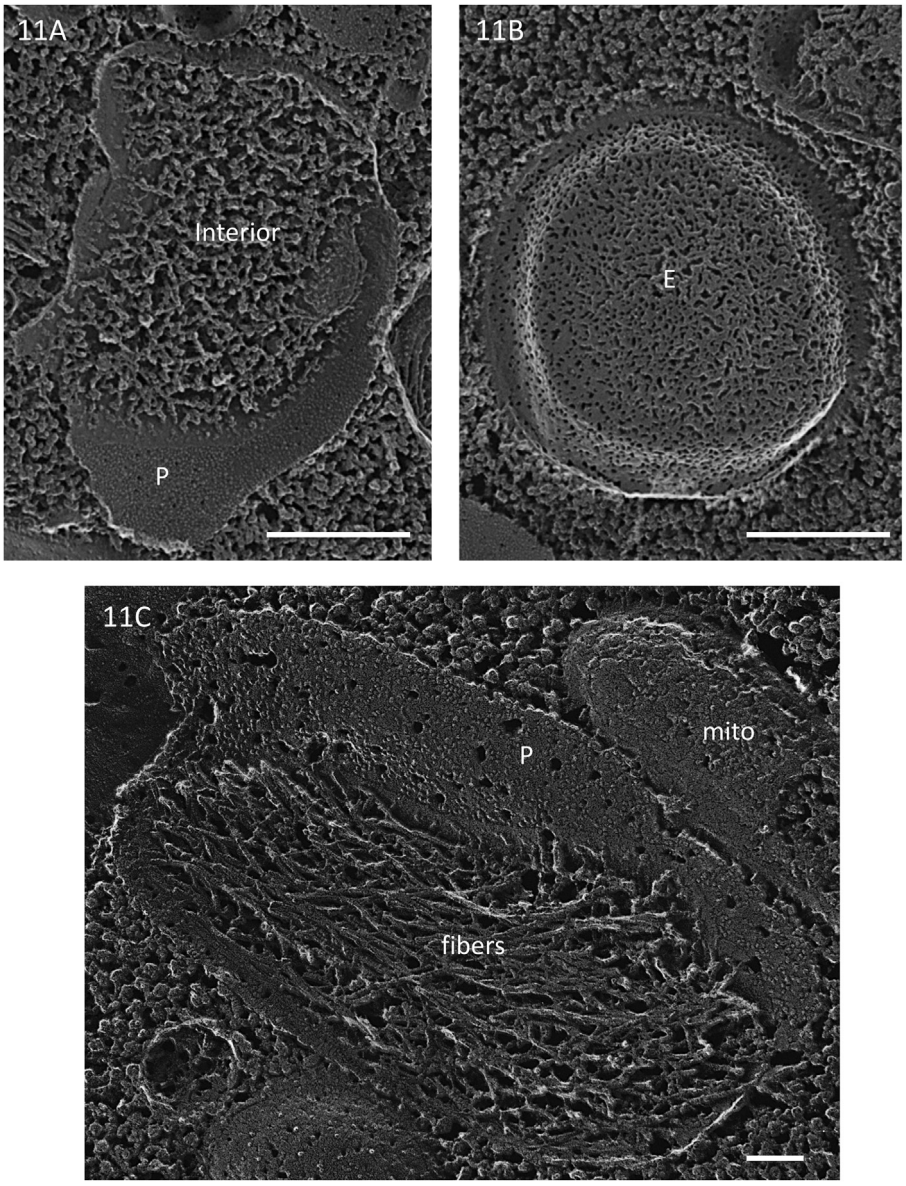

Figure 11. Log-phase vacuoles. (**A**) Vacuole interior of log-phase *sta6* grown in P-buffered medium showing granular interior contents and small IMPs of P-face. Bar, 500 nm. (**B**) Pitted E-face of vacuole from log-phase *sta6*. Bar, 500 nm. (**C**) Vacuole interior of log-phase *sta6* grown in Tris-buffered medium showing fibers in the interior and small IMPs of P-face. Mito, mitochondrion. Bar, 100 nm.

Acidocalcisomes are encountered more frequently in some organisms than others, but since only *C. reinhardtii* was sampled heavily, and most organisms were harvested from a single growth condition, sampling may have been biased. The organelles are of a similar size (400–600 nm) in most species but are uniformly small (~200 nm) in *T. brucei* procyclic forms (Supplementary Material Fig. S9).

Seufferheld et al. (2003, 2004, 2011) report that polyphosphate granules in several bacteria are surrounded by a membrane, and suggest that acidocalcisomes have an ancient bacterial origin (reviewed in Grant et al. 2018). Supplementary Material Figure S10 shows cisternal membrane cross-sections (A) and vesicular membrane fracture faces (B) within one of these bacteria, *Agrobacterium tumefaciens*; such internal

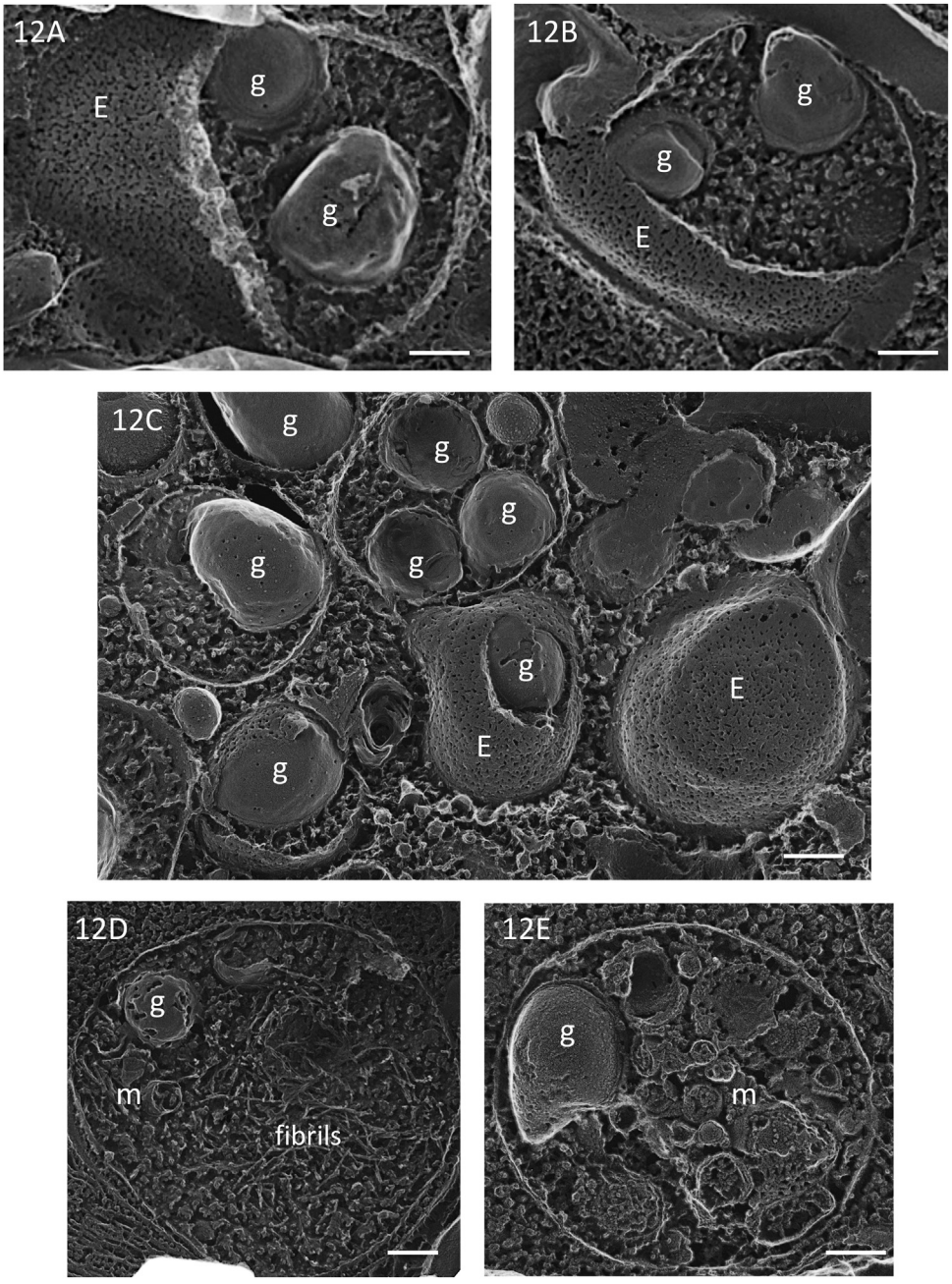

Figure 12. Autophagocytic vacuoles containing polyphosphate granules. E, E-face; g, polyphosphate granule; m, membranous material. (**A**) *sta6* 96 h N-starve from log phase. Bar, 250 nm. (**B**) *sta6* 10 days N-starve from log phase. Bar, 250 nm. (**C**) *sta6* 10 days N-starve from log phase. Bar, 200 nm. (**D**) *sta6* grown in Tris-buffered media, stationary phase. Bar, 200 nm. (E) *sta6* stationary phase. Bar, 250 nm.

membrane profiles are not evident in numerous other bacteria imaged in our laboratory. No cross-fractured images containing granules were encountered, albeit these are also infrequently encountered in eukaryotes.

Phylogenetics of the Acidocalcisome-resident H^+-PPase Pump

Given our ultrastructural evidence for a widespread distribution of acidocalcisomes, we undertook an in-depth analysis of 86 eukaryotic PPase

sequences from numerous radiations, using the *C. reinhardtii* homolog (Cre09.g394436) of EC 3.6.1.1 in a BLAST search supplemented with searches of individual genomes/transcriptomes. Supplementary Material Tables S2 and S3 present the data, Supplementary Material Figure S11 shows our sequence alignments, and Figure 13 shows a tree generated from a maximum-likelihood analysis of these alignments.

The usual range of E-values is $<10^{-70}$, reflecting the very strong conservation throughout the 15-16 transmembrane domains and the cytoplasmic/interior loops (Supplementary Material Fig. S11). Indeed, when we constructed trees using just the transmembrane or just the loop domains (following the topology predicted in McIntosh and Vaidya (2002)), we obtained the same tree configuration as with the whole protein.

We confirmed the prior report of two gene/pump "subclasses" in eukaryotes (McIntosh and Vaidya 2002), and detected a third subclass in genomes that the earlier study did not query. We designate these eukaryotic subclasses as Clades 1-3 (Fig. 13).

Further analyses were informed by an important study by Luoto et al. (2011). They distinguished prokaryotic (bacterial and archaeal) PPase pumps as being either K^+-independent (four clades, designated P1-P4 in Fig. 13) or K^+-dependent (four clades, designated PA-PD in Fig. 13, with clade D differentiating into subclades PD1-PD3). They further documented, using in vitro assays, that three of the six K^+-dependent groupings (PB, PC, and PD1) encode Na^+ pumps and not H^+ pumps. Their data indicate that the K^+-independent pump was ancestral and that the K^+-dependent H^+-pump evolved from the K^+-dependent Na^+-pump. The few eukaryotic PPases queried in their study were found to be homologous to either the K^+-independent P3 group or the K^+-dependent PD3 group.

Using their sequence criteria for pump classification (amino-acid positions #478-481; Supplementary Material Fig. S11), we found that our Clade 1 genes are homologous to the prokaryotic K^+-dependent H^+-PPases, most closely to the PD3 group; our Clade 2 genes are most closely related to the prokaryotic K^+-independent H^+-PPases; and our Clade 3 genes are most closely related to the prokaryotic K^+-dependent Na^+-PPases (an activity that has not yet been demonstrated experimentally in eukaryotic studies).

We also queried five PPases from the Asgard archaeal group that is reported to have eukaryotic features (Zaremba-Niedzwiedzka et al. 2017). All were scored as K^+-independent, and one, OLS24026, clusters with the eukaryotic K^+-independent Clade 2 (Fig. 13, red asterisk) with very strong support.

Homologs of all three clades are present in all the major eukaryotic super groups queried (Supplementary Material Table S2), suggesting that all were present in the LECA genome, but there is no obvious phylogenetic pattern in their modern distribution (Fig. 13 and Supplementary Material Table S2).

Of the eukaryotic genomes queried, 42% encode only one PPase, 34% encode two, and 24% encode three to five, where a given clade may have more than one representative per genome (Supplementary Material Table S2). For example, Supplementary Material Figure S12 shows alignments of the five genes encoded by the green prasinophyte *Cymbomonas*, with three similar Clade-1 sequences and distinctive Clade-2 and Clade-3 sequences.

Using the phylogenetic tree of Brown et al. (2018) for taxonomic reference, the PPase sequence is absent from Amoebozoa and from the opisthokont branch of Obazoa (e.g. *Fonticula* (a non-Amoebozoan cellular slime mold), *Salpingoeca* and *Monosiga* (choanoflagellates), *Capsapora* (Filasterea), and *Sphaeroforma* (Ichthyosporea)). It is, however, present in the two other branches of Obazoa: Apusomonada (*Thecamonas trahens* and *Amastigomonas* sp) and Breviatea (*Pysguia biforma*). It is also present in two radiations posited to have branched between the root of the eukaryotic tree and Obazoa + Amoebozoa: Malawimonadidae (*Gefionella okellyi*; Heiss et al. 2018), and Ancyromonadida (*Ancyromonas sigmoides*; Brown et al. 2018). QFDEEM images of candidate acidocalcisomes have been found in the apusomonad *Chelonemonas* (Goodenough and Heiss, unpublished). Hence the PPase pump, and likely the acidocalcisome, appears to have been lost in the opisthokonts and the Amoebozoa, albeit, as noted in the Introduction, "lysosome-related organelles," lacking the pump, have been identified in several animals.

Homologs are present in the Discoba branch of the "excavates" (*Naegleria*, *Trypanosoma*, *Euglena*) and in one member of the Metamonada branch (*Trimastix marina*), but none were detected in two other metamonads (*Giardia lamblia* and *Trichomonas vaginalis*), presumably due to gene loss.

The absence of the gene from queried Amoebozoa, including two *Dictyostelium* species (Supplementary Material Table S3), is at odds with the reported H^+-PPase activity in *D. discoideum*

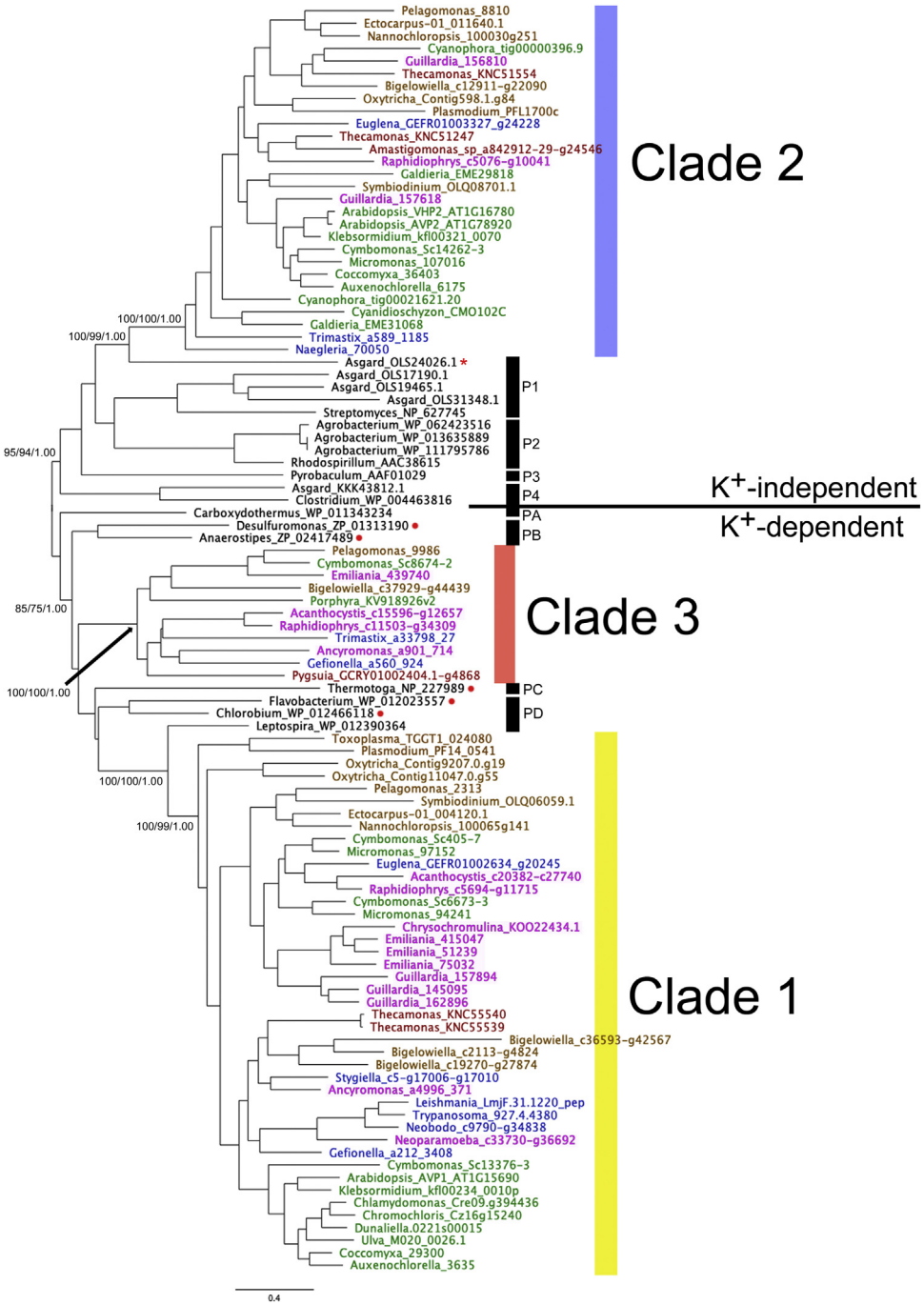

Figure 13. Maximum likelihood (ML) phylogeny of the H^+-PPase in eukaryotes. The ML trees were generated from the full-length alignment (Supplementary Material Fig. S11) with 692 amino acid positions. The best tree is shown. The three numbers at critical nodes show %bootstrap, %SH-aLRT score, and Bayesian posterior probability in support of clades. The tree contains 14 bacterial sequences and five Asgard archaeal sequences marked by black vertical bars as outgroup. Clade information for prokaryotic sequences derives from Luoto et al. (2011). Colored vertical bars on the right depict the three proposed clades: Clade 1 in yellow, Clade 2 in blue, and Clade 3 in red. Sequence names are colored by their taxonomic groups: green for Archaeplastida, brown for SAR (Stramenopiles, Alveolata, Rhizaria), blue for "Excavata", red for Amorphea, and magenta for "Other". Red dots following sequence names indicate experimentally verified sodium-specific PPase pumps (Luoto et al. 2011). Asterisk: Asgard member of Clade 2. Details of the sequences analyzed in this phylogeny

(Marchesini et al. 2002), a discrepancy that merits investigation.

Discussion

The five hallmarks of an acidocalcisome, reviewed in the Introduction, are not unique to these organelles. 1) Its polyphosphate polymers are found throughout the biological kingdom as well as in ancient ocean deposits. 2) Its polyphosphate granules are also found in bacteria and platelets. 3) Its signature H^+-PPase pump is present in bacteria (although not cyanobacteria) and archaea, has been retained by land-plant (but not fungal) vacuoles, and is reported to localize as well in non-acidocalcisomal protist membranes (Martinez et al. 2002; Miranda et al. 2010; Rohloff et al. 2004). 4) Its V-type ATPase, cation transporters/exchangers, and aquaporins are found in numerous other locations. 5) Its acidic internal pH is shared with fungal and land-plant vacuoles and animal endosomes/lysosomes/secretory compartments. The distinctiveness of acidocalcisomes is that these features are brought together in a single organelle.

That acidocalcisomes serve as storage organelles for (poly)phosphate and various cations is well documented, and the finding that their loss compromises the infectious cycle of human parasites suggests that they may perform additional functions that await identification. Askoy et al. (2014), for example, document that in *C. reinhardtii*, deletion of the *VTC1* gene, one of four subunits of the VTC complex that associates with acidocalcisomes and catalyzes polyphosphate polymerization, results in a complex phenotype including, as expected, compromised polyphosphate content but also defective vacuole formation and hyper-sensitivity to stress conditions. We have identified at least one acidocalcisome morphological variant, the "double decker," in *C. reinhardii* and *T. brucei* (Figs 1 and 3 and Supplementary Material Fig. S8I), suggesting that there may prove to be several acidocalcisome classes with diverse functions.

Acidocalcisome Membranes

We report an apparently unique hallmark of the acidocalcisome, namely, the distinctive ultrastructural properties of its surrounding membrane. The fracture faces of all membranes types are known to cavitate in a distinctive fashion with etching, where variables presumably include transmembrane protein content/density, water content, and lipid composition. That said, the cavitation pattern of the acidocalcisome E-face is highly unusual, shifting from smooth (non-etched) to rugose (etched), setting it apart from all other membranes evaluated in our laboratory. The P-face is also distinctive, with a strikingly dense population of small IMPs that often align in rows. Both faces, particularly the E-face, are often delimited by a flattened rim, possibly generated by the cytoplasmic domains of its constituent pumps and transporters.

Particularly intriguing is the shift in etched-E-face organization from rugose to densely packed arrays of discrete ~14-nm globular domains, observed once in situ (Fig. 8C and D) and once when log-phase acidocalcisomes were released into a mannitol solution from digitonin-ruptured cells (Fig. 9). Since no other membranes in the preparation displayed this phenotype, it reflects a unique property of the acidocalcisome membrane and not some generalized response to the breakage procedure. The images are consistent with the hypothesis that intramembranous globular domains in log-phase organelles usually become melded together into the rugose configuration during the etching process.

Numerous proteins span acidocalcisomal membranes in the trypanosomatids (Docampo and Huang 2016), including cation exchangers/transporters, the polyphosphate polymerase subunit of the VTC protein, and two proton pumps – the distinctive H^+-PPase and the widely-distributed V-type ATPase. The H^+-PPase is predicted to be a homodimer with 16 transmembrane domains in each subunit (McIntosh and Vaidya 2002). The V-type pump has a membrane-integral domain, V_0 (Casey et al. 2010), through which protons pass, and a peripheral rotating V_1 domain carrying out the ATPase activity. The V_0 domain has been shown to form a 12-nm particle (Henderson et al. 2011), comparable in size to the 14-nm globular domains seen in the cell-free log-phase acidocalcisome membranes; the size of the 32-transmembrane-domain H^+-PPase dimer has not been reported but is also expected to be large.

are provided in Supplementary Material Table S2. (For interpretation of the references to color in this figure legend, the reader is referred to the web version of this article.)

Acidocalcisome Membrane Universality

Polyphosphate-containing organelles have been previously detected by light or electron microscopy in the following eukaryotic microbes: 1) parasitic protists such as *T. brucei* and *Toxoplasma gondii* (reviewed in Docampo 2016; Docampo and Huang 2016); 2) green algae (*Dunaliella* salina: Pick and Weiss 1991; *Tetraselmis subcordiformis*: Salisbury 1982; *Desmodesmus*: Shebanova et al. 2017; *C. reinhardtii*: Komine et al. 1996, 2000; Ruiz et al. 2001a; Hong-Hermesdorf et al. 2014; Askoy et al. 2014: *C. eugametos*/*moewusii*: Lewin 1952, Siderius et al. 1996; and lichen photobionts: Guschina et al. 2003); 3) red algae (Nagasaka et al. 2003; Yagisawa et al. 2009); 4) stramenopiles (Karlson et al. 1996); and 5) the Amoebozoan slime mold *Dictyostelium discoideum* (Marchesini et al. 2002). The current study covers and expands this inventory to include additional green algae, several secondary-symbiotic algae, and the "excavate" amoeba-flagellate *Naegleria gruberi* (Supplementary Material Figs S6-S9). Few examples of cross-fractured granule-containing organelles were encountered in this survey, which is also the case for the deeply sampled *C. reinhardtii*, but the smooth → rugose E-face and the concave IMP-dense P-face, often with rims, are diagnostic across phyla.

Acidocalcisome Biogenesis in the Golgi

Whereas most eukaryotic organelles are generated by expansion and division of pre-existing organelles, the acidocalcisome is apparently assembled de novo at the trans-face of the Golgi in *C. reinhardtii* and *T. brucei* (Fig. 10), receiving input from Golgi-derived vesicles, as are lysosome-related organelles (Raposo et al. 2007). Acidocalcisome biogenesis in parasites requires the clathrin-adaptor AP3 protein, involved in targeting membrane and cargo to Golgi-derived compartments (Besteiro et al. 2008; Huang et al. 2011; Li and He 2014), further underscoring a Golgi origin, albeit a gene encoding AP3 has yet to be annotated in *C. reinhardtii*.

Acidocalcisomes and Vacuoles in *C. reinhardtii*

Log-phase *C. reinhardtii* cells produce acidocalcisomes, recognized by their rugose E-face morphology, that only rarely contain polyphosphate granules. Log-phase cells also produce small, granule-free cytoplasmic vacuoles with non-rugose E-faces (Fig. 11B; Supplementary Material Fig. S5E and F) which accumulate fibers when the cells are grown in Tris-buffered media (Fig. 11C; Supplementary Material Fig. S5A and B).

Under stress conditions, granules are found in both acidocalcisomes and vacuoles. The stress-associated vacuoles commonly contain membrane debris as well, leading us to designate them as autophagy-related vacuoles, and they often contain two or more granules (Fig. 12 and Supplementary Material Fig. S5E and F); by contrast, stressed acidocalcisomes contain only one granule and no debris. That the autophagy-related vacuoles derive from log-phase vacuoles is indicated by the presence of Tris-induced fibers in both (Fig. 12D and Supplementary Material Fig. S5A and B).

Many of the published images of large granule-containing compartments in stressed *C. reinhardtii* cells likely illustrate autophagy-related vacuoles and not acidocalcisomes. Hong-Hermesdorf et al. (2014) document that such vacuoles in Zn-limited cells have an acidic internal pH, and that granules are often released from such cells into the confines of the cell wall by exocytosis (images absent from our collection since we usually studied wall-less cells that would not retain released granules).

Left unexplained is how the granules move from an acidocalcisomal to a vacuolar compartment. An attractive hypothesis is that acidocalcisomes fuse with existing cytoplasmic vacuoles under stress conditions, releasing their granules and soluble enzymes into the vacuolar lumen and delivering acidifying pumps and channels to the vacuolar membrane. Support for this hypothesis comes from *T. brucei* and *T. cruzi*: 1) acidocalcisomes are reported to fuse with contractile-vacuole membranes (Rohloff et al. 2004); 2) the induction of autophagy and autophagosome formation by N-starvation is accompanied by an increased acidocalcisomal acidification (Li and He 2014); and 3) treatments that inhibit acidocalcisome biogenesis or that cause acidocalcisome alkalinization result in autophagy inhibition (Li and He 2014). Tests of this hypothesis using tagged organelles will hopefully be conducted in the future.

The Physical States of Polyphosphate in Acidocalcisomal and Vacuolar Compartments

Polyphosphates exist in four interconvertible physical states (Ando et al. 2010; Moreno et al. 2002; Nikolić et al. 2016; Omelon and Grynpas 2008): 1) water-soluble; 2) suspended as a sol; 3) condensed as a gel; or 4) glass-like (e.g. the polyphosphate particulates used in commercial water filtration systems to remove metals.) Variables that influence these configurations include temperature, polymer chain length and concentration, pH, and levels of chelated cations, which

promote both polymerization and condensation (water loss) (Klompmaker et al. 2017). The concentration and chain-lengths of polyphosphates contained within membrane compartments, like acidocalcisomes and vacuoles, are also influenced by cation transporters and by polyphosphate phosphatase and kinase/polymerase activities. Cellular transitions between these various physical states are therefore expected to be under complex regulation.

In TEM images of thin-sectioned cells, short-chain-length polyphosphates in solution or longer polymers in suspension are not expected to block the electron beam; hence the electron-dense material within membrane enclosures in these images (e.g. Fig. 1) presumably represents long-chain polyphosphate in a gel or solid configuration. This material can take the form of discrete, sharp-edged granules, presumably solid, that separate from the membrane (Guschina et al. 2003; Komine et al. 2000; Medeiros et al. 2011; Miranda et al. 2008; Scott et al. 1997; Yagisawa et al. 2009; Fig. 1), or it can appear gel-like, either filling the enclosure or forming irregular islands that often adhere to the membrane at the vesicle perimeter (De Jesus et al. 2010; Docampo and Huang 2015, 2016; Karlson et al. 1996; Penen et al. 2017; Pick and Weiss 1991; Salisbury 1982; Shebanova et al. 2017; Siderius et al. 1996; Vannier-Santos et al. 1999; Yagisawa et al. 2007). While such variation may in some cases be due to specimen preparation techniques (Docampo et al. 2005), we suggest that it also reflects bona fide differences in physical states. For example, Supplementary Material Figure S13 shows a survey of N-starved cells with both granular and irregular (arrows) electron-dense inclusions, and figure 5a of Hong-Hermesdorf et al. (2014) shows a Zn-depleted cell whose electron-dense material adopts two configurations: granules that are undergoing exocytosis into the neutral-pH periplasm, and irregular islands that fill the acidic-pH vacuoles.

During the QFDEEM procedure, polyphosphate sols would be etched and collapse, meaning that only solid granules or dense gels would be identifiable in replicas. Granules are present in replicas of stressed but not in unstressed acidocalcisomes in *C. reinhardtii*, and they disappear when stressed cells are transferred to growth conditions. Moreover, the acidocalcisomes in cells imaged shortly after transfer (Supplementary Material Fig. S4) contain granules with irregular edges, or homogenous material that fills the lumen, or coarse aggregates, suggestive of changes in physical state.

We also report RNA-seq analyses of *C. reinhardtii* cells subjected to two stress conditions. In contrast to autophagy-related genes whose expression is amplified by stress, transcript levels of the *AVP1* (H^+-PPase) gene decrease 2-4 fold under both conditions (Supplementary Material Table S1). This pattern is consistent with a scenario wherein, under stress conditions, the acidocalcisome interior becomes less acidic and hence more prone to forming long-chain polyphosphate and chelating cations.

Collectively, these observations are consonant with the following proposal for *C. reinhardtii*. 1) Unstressed (log-phase) cells maintain an acidic lumen in their acidocalcisomes that favors soluble short-chain polyphosphates, in turn favoring PPi liberation by resident or local polyphosphatases. The PPi powers the H^+-PPase pump, helping to maintain the low pH and allowing the acid-dependent exchangers/transporters in the organelle membrane to import Ca^{++} and metals in exchangeable forms available for growth. A caveat here is that the PPi-hydrolyzing domain of the pump faces the cytoplasm and no transporter has yet been identified that carries PPi from the acidocalcisome lumen to the cytoplasm. 2) In stressed cells, pump levels decrease and PPi polymerization is favored, depleting the pump of substrate and hence increasing the internal pH which stimulates further polymerization and further alkalinization, the end result being the condensation of polyphosphates into electron-dense gels and granules. These serve to sequester calcium and metals, including toxic metals, and the cations, in turn, further promote polymerization (Klompmaker et al. 2017), the process being reversible with stress alleviation. Such a system might be unique to *C. reinhardtii* or might also pertain to other organisms, where the reported alkali-stimulation of recombinant PPase activity in *T. cruzi* (Galizzi et al. 2013) is inconsistent with this model.

Distribution of H^+-PPase-encoding Genes in Eukaryotes

Identification of the eukaryotic H^+-PPase-encoding protein, a hallmark of acidocalcisomes, is facilitated by the strong full-length conservation of its amino-acid sequence (Supplementary Material Fig. S11). Its inclusion in 40 widely dispersed eukaryotic genomes/transcriptomes (Supplementary Material Table S2 and Fig. 13) documents its ubiquity, and its loss in opisthokonts and Amoebozoans is notable. Interestingly, the gene is present in four lineages (Apusomonada, Breviatea, Malawimonadidae, and

Ancyromonadida) that are posited by some investigators to branch adjacent to opisthokonts (Brown et al. 2018), possibly pinpointing this loss to an important juncture in evolutionary history.

We confirm and expand the finding (McIntosh and Vaidya 2002) that the conserved eukaryotic sequence partitions into two subclasses, and we report a third subclass in eukaryotic genomes not covered in their study. We designate these as Clades 1-3 (Fig. 13). Strikingly, there is no obvious correlation between taxonomy and clade distribution (Fig. 13 and Supplementary Material Table S2): each clade populates numerous radiations. This suggests that the founders of all three clades were present in the LECA and persisted during the early diversification of eukaryotic lineages, followed by selective loss/retention. The loss/retention process has apparently continued throughout the span of eukaryotic evolution since it can even be observed in some sister lineages: for example, the closely related apicomplexans *Plasmodium falciparum* and *Toxoplasma gondii* encode near-identical Clade-1 genes, but *Plasmodium* also carries a Clade-2 gene that is absent from *Toxoplasma*. In such cases, clade endowment may prove to be a useful small-scale lineage marker.

Since *C. reinhardtii* and *T. brucei* each encodes only a single Clade-1 gene and since their isolated acidocalcisomes possess H^+-PPase activity, it can be assumed that the Clade-1 protein is acidocalcisome-associated in these organisms. Otherwise, it is not known whether Clade-2 and Clade-3 pumps also associate with acidocalcisomes and/or acidocalcisomal variants, nor whether they (and Clade 1) also localize to additional membrane types. Also untested is whether some of the eukaryotic proteins designated herein as H^+-PPases are in fact Na^+-PPases, as is the case for a subset of bacterial members of the family (Luoto et al. 2011). Three studies report pump activity in eukaryotic non-acidocalcisomal locations (Martinez et al. 2002; Miranda et al. 2010; Rohloff et al. 2004), consonant with the possibility that different pump subtypes, perhaps in combination, service distinctive membrane systems.

Methods

Strains: *C. reinhardtii* strains CC-620 (wild-type), CC-4349 (*cw15*) and CC-4348 (*sta6*) were grown mixotrophically (acetate-supplemented) in phosphate-buffered (Sueoka 1960) or Tris-buffered (Gorman and Levine 1965) media and were visualized in log-phase or stationary-phase or following nitrogen (N)-starvation. Growth conditions are described in Goodson et al. (2011). *Cyanidioschyzon merolae* was grown in the Goodenough lab as described (Kobayashi et al. 2010). All other organisms were grown in the laboratories of collaborators, listed in Acknowledgements, and directly provisioned or overnight-shipped to St. Louis for freezing.

Quick-freeze deep-etch electron microscopy: Pelleted live microorganisms were placed on a cushioning material and dropped onto a liquid-He-cooled copper block; the frozen material was transferred to liquid nitrogen and fractured under vacuum, etched at −80 °C for 2 min (or 1 min for "lightly etched") and Pt/C rotary-replicated under vacuum as described (Heuser 2011). Replicas were examined with a JEOL electron microscope, model JEM 1400, equipped with an AMTV601 digital camera. The images are photographic negatives; hence protuberant elements of the fractured/etched surface are most heavily coated with platinum and appear white.

Quick-freeze freeze-substituted electron microscopy: Samples were prepared as described in Heuser (2011).

Digitonin/mannitol cell breakage: Following an earlier protocol developed to isolate intact chloroplasts (Klein et al. 1983), either log-phase or stationary-phase *sta6* cells were harvested, resuspended in 40 ml of digitonin solution (5 mM potassium-phosphate buffer pH 6.5, 6% PEG 6000, 0.004% digitonin, 1 mM PMSF), transferred to a cold metal beaker and heated to 27 °C in a 48 °C water bath with constant swirling. Once 27 °C was reached, the suspension was transferred to a 30 °C shaking water bath, shaken for 10 min, centrifuged at 1,000 g for 5 min, resuspended in 10 ml of mannitol buffer (20 mM HEPES-NaOH pH 7.7, 0.15 M mannitol, 1 mM $MgCl_2$, 2 mM EDTA, 1 protease inhibitor tablet (Roche Complete Ultra Mini)) and then centrifuged at 10,000 *g* for 30 min prior to freezing the pellet.

RNA-Seq analysis: Protocols and data for the N-starvation experiments are published in Goodenough et al. (2014). Similar protocols were used for stationary-phase experiments with either *sta6* grown mixotrophically or the CC-1690 (21gr) wild-type strain grown phototrophically with a 0.5% CO_2 supplement. A full report of these experiments is in preparation.

Phylogenetic reconstruction of H^+-PPase: Eukaryotic homologs were searched by BLASTP using the *Chlamydomonas AVP1* gene as the query sequence; eight outgroup prokaryotic sequences were recovered from the Genbank nr database or from Asgard archaea sequences (Zaremba-Niedzwiedzka et al. 2017). The E-values of the collected eukaryotic homologs were $\leq 10^{-30}$ (Supplementary Material Table S2).

Genomes lacking a sequence with an E-value $\leq 10^{-2}$ were scored as containing no homolog (Supplementary Material Table S3). To verify their absence in opisthokonts and Amoeobozoa, we queried the Apusomonadida sequences and failed to collect any homologues. After excluding eight partial or highly divergent sequences, the remaining sequences were aligned using the MAFFT algorithm. The final alignment used for phylogenetic analysis was made by excluding gaps present in >50% of sequences, containing 692 sites with 90 entries (Supplementary Material Fig. S11). A phylogenetic reconstruction was performed using maximum-likelihood methods (IQ-TREE; Minh et al. 2013). The LG + F + R7 model was chosen according to Bayesian Information Criteria (Luo et al. 2010). Branch support scores were collected by 'Ultrafast' bootstrapping with the '-bb 2000 −bi 500' options (Minh et al. 2013), Shimodaira-Hasegawa-like (SH) aLRT test values with '-alrt 1000' option, and Bayesian approximate likelihood-ratio tests with '-abayes' option, performed by IQ-TREE (Anisimova et al. 2011).

Declarations of Interest: None.

Acknowledgements

We are most grateful to the laboratories that provided us with the following organisms: *Agrobacterium tumifaciens*, Lucia Strader, Washington University; *Asterochloris glomerata*, Daniele Armaleo, Duke University; *Auxenochlorella protothecoides*, Richard Sayre, Los Alamos National Laboratories; *Botryococcus braunii*, Timothy Devarenne, Texas A&M University; *Chlamydomonas monoica*, Karen Vanwinkle-Swift, Northern Arizona University; *Chroomonas mesostigmatica*, John Archibald, Dalhousie University; *Cyanidioschyzon merolae,* Mio Ohnuma, Rikkyo University; *Cyanophora paradoxa* Debashish Bhattacharya, Rutgers University; *Cyclotella cryptica*, Mark Hildebrand, UC San Diego; *Dunaliella salina* and *Haematococcus* sp, Juergen Polle, Brooklyn College; *Galdieria sulphuraria*, Peter Lammers, Arizona State University; *Naegleria gruberi*, Chandler Fulton, Brandeis University; *Nannochloropsis gaditana*, Matthew Posewitz, Colorado School of Mines; *Nannochloropsis oceanica*, Christoph Benning, Michigan State University; *Neospora caninum*, David Sibley, Washington University; *Phaeodactylum tricornutum* and *Pelagomonas calceolata*, Andrew Allen and Christopher Dupont, J Craig Venter Institute; *Polytomella parva*, Robert Lee, Dalhousie University; *Symbiodinium* CD1576, Robert Blankenship, Washington University; *Trypanosoma brucei*, Roberto Docampo, University of Georgia. The freeze-substituted thin sections and anaglyph images (Fig. 1 and Supplementary Figs. S1, S2 and S13) were provided by John Heuser (National Institute of Child Health and Human Development). Stimulating conversations with Roberto Docampo (University of Georgia) greatly improved our understandings of these organelles.

Funding for this project was provided by the US Department of Energy and by the International Center for Energy, Environment and Sustainability to UG, by Discovery Grant 418471-12 from the Natural Sciences and Engineering Research Council (NSERC) to JL, by the Korea CCS R&D Center (KCRC), Korean Ministry of Science, grant no. 2016M1A8A1925345 to JL, and by a grant (#382790) from the Simons Foundation to AAH. Funding sources played no role in the contents of this report.

Appendix A. Supplementary Data

Supplementary data associated with this article can be found, in the online version, at https://doi.org/10.1016/j.protis.2019.05.001.

References

Achbergerova L, Nahalka J (2011) Polyphosphate – an ancient energy source and metabolic regulator. Microb Cell Fact **10**:63

Ando M, Imadzu S, Kitagawa S, Ohtani H (2010) Crystallization efficiencies of inorganic polyphosphate oligomers reacted with magnesium and calcium cations using anion-exchange chromatography with particulate formation-laser scattering detector. J Chromatogr A **1217**:5298–52301

Anisimova M, Gil M, Dufayard J-F, Dessimoz C, Gascuel O (2011) Survey of branch support methods demonstrates accuracy, power, and robustness of fast likelihood-based approximation schemes. Syst Biol **60**:685–699

Armbrust EV, Ibrahim A, Goodenough UW (1995) A mating type-linked mutation that disrupts the uniparental inheritance of chloroplast DNA also disrupts cell-size control in *Chlamydomonas*. Mol Biol Cell **6**:1807–1818

Asaoka M, Segami S, Maeshima M (2014) Identification of the critical residues for the function of vacuolar H^+-pyrophosphatase by mutational analysis based on the 3D structure. J Biochem **156**:333–344

Askoy M, Pootakham W, Grossman AR (2014) Critical function of a *Chlamydomonas reinhardtii* putative polyphosphate polymerase subunit during nutrient deprivation. Plant Cell **26**:4214–4229

Au KM, Barabote RD, Hu KY, Saier MH Jr (2006) Evolutionary appearance of H+-translocating pyrophosphateses. Microbiology **152**:1243–1247

Azevedo C, Saiardi A (2017) Eukaryotic phosphate homeostasis: the inositol pyrophosphate perspective. Trends Biochem Sci **42**:219–231

Besteiro S, Tonn D, Tetley L, Coombs GH, Mottram JC (2008) The AP3 adaptor is involved in the transport of membrane proteins to acidocalcisomes of *Leishmania*. J Cell Sci **121**:561–570

Blaby-Haas CE, Merchant SS (2017) Regulating cellular trace metal economy in algae. Curr Opin Plant Biol **39**:88–96

Brown MRW, Kornberg A (2004) Inorganic polyphosphate in the origin and survival of species. Proc Natl Acad Sci USA **101**:16085–16087

Brown MW, Heiss AA, Kamikawa R, Inagaki Y, Yabuki A, Tice AK, Shiratori T, Ishida K-I, Hashimoto T, Simpson AGB, Rogers AJ (2018) Phylogenomics places orphan protistan lin-

eages in a novel eukaryotic super-group. Genome Biol Evol **10**:427–433

Casey JR, Grinstein S, Orlowski J (2010) Sensors and regulators of intracellular pH. Nature Rev Mol Cell Biol **11**:50–61

Cordeiro CD, Saiardi A, Docampo R (2017) The inositol pyrophosphate synthesis pathway in *Trypanosoma brucei* is linked to polyphosphate synthesis in acidocalcisomes. Mol Microbiol **106**:319–333

Da Silva LM, Beverly SM (2010) Expansion of the target of rapamycin (TOR) kinase family and function in *Leishmania* shows that *TOR3* is required for acidocalcisome biogenesis and animal infectivity. Proc Natl Acad Sci USA **107**:11965–11970

De Jesus TCL, Tonelli RR, Nardelli SC, Augusto LS, Motta MCM, Girard-Dias W, Miranda K, Ulrich P, Jimenez V, Barquilla B, Navarro M, Docampo R, Schenkman S (2010) Target of rapamycin (TOR)-like 1 kinase is involved in the control of polyphosphate levels and acidocalcisome maintenance in *Trypanosoma brucei*. J Biol Chem **285**:24131–24140

Desfougères Y, Gerasimait. e R, Jessen HJ, Mayer A (2016) Vtc5, a novel subunit of the vacuolar transporter chaperone complex, regulates polyphosphate synthesis and phosphate homeostasis in yeast. J Biol Chem **291**:22262–22275

Diaz J, Ingall E, Benitez-Nelson C, Paterson D, de Jonge MD, McNulty I, Brandes JA (2008) Marine polyphosphate: a key player in geologic phosphorus sequestration. Science **320**:652–655

Docampo R (2016) The origin and evolution of the acidocalcisome and its interactions with other organelles. Mol Biochem Pharmacol **209**:3–9

Docampo R, Huang G (2015) Calcium signaling in trypanosomatid parasites. Cell Calcium **57**:194–202

Docampo R, Huang G (2016) Acidocalcisomes of eukaryotes. Curr Opin Cell Biol **41**:66–72

Docampo R, Moreno S (2008) The acidocalcisome as a target for chemotherapeutic agents in protozoan parasites. Curr Pharm Des **14**:882–888

Docampo R, de Souza W, Miranda K, Rohloff P, Moreno SNJ (2005) Acidocalcisomes – Conserved from bacteria to man. Nat Rev Microbiol **3**:251–261

Drozdowicz YM, Shaw M, Nishi M, Striepen B, Liwinski HA, Roos DS, Rea PA (2003) Isolation and characterization of TgVP1, a Type I vacuolar H+-translocating pyrophosphatase from *Toxoplasma gondii*. J Biol Chem **278**:1075–1088

Fang J, Rohloff P, Miranda K, Docampo R (2007) Ablation of a small transmembrane protein of *Trypanosoma brucei* (TbVTC1) involved in the synthesis of polyphosphate alters acidocalcisome biogenesis and function, and leads to a cytokinesis defect. Biochem J **407**:161–170

Gal A, Sorrentino A, Kahil K, Pereiro E, Faivre D, Scheffel A (2018) Native-state imaging of calcifying and noncaldifying microalgae reveals similarities in their calcium storage organelles. Proc Natl Acad Sci USA **115**:11000–11005

Galizzi M, Bustamante JM, Fang J, Miranda K, Medeiros LCS, Tarleton RL, Docampo R (2013) Evidence for the role of vacuolar soluble pyrophosphatase and inorganic polyphosphate in *Trypanosoma cruzi* persistence. Mol Microbiol **90**:699–715

Gerasimaitè R, Mayer A (2017) Ppn2, a novel Zn^{2+}-dependent polyphosphatase in the acidocalcisome-like yeast vacuole. J Cell Sci **130**:1625–1636

Goodenough U, Blaby I, Casero D, Gallaher SD, Goodson C, Johnson S, Lee J-H, Merchant SS, Pellegrini M, Roth R, Rusch J, Singh M, Umen JG, Weiss TL, Wulan T (2014) The path to triacylglyceride obesity in the *sta6* strain of *Chlamydomonas reinhardtii*. Eukaryot Cell **13**:591–613

Goodson C, Roth R, Wang ZT, Goodenough U (2011) Structural correlates of cytoplasmic and chloroplast lipid body synthesis in *Chlamydomonas reinhardtii* and stimulation of lipid body production with acetate boost. Eukaryot Cell **10**:1592–1606

Gorman DS, Levine RP (1965) Cytochrome f and plastocyanin: their sequence in the photosynthetic electron transport chain of *C. reinhardi*. Proc Natl Acad Sci USA **54**:1665–1669

Grant CR, Wan J, Komeili A (2018) Organelle formation in bacteria and archaea. Annu Rev Cell Dev Biol **34**, 19.1–19.22

Guschina IA, Dobson G, Harwood JL (2003) Lipid metabolism in cultured lichen photobionts with different phosphorus status. Phytochemistry **64**:209–217

Heiss AA, Kolisko M, Ekelund F, Brown MW, Roger AJ, Simpson AGB (2018) Combined morphological and phylogenomic re-examination of malawimonads, a critical taxon for inferring the evolutionary history of eukaryotes. Roy Soc Open Sci **5**:171707

Henderson R, Chen A, Chen JZ, Grigorieff N, Passmore LA, Ciccarelli L, Rubinstein JL, Crowther RA, Stewart PL, Rosenthal PB (2011) Tilt-pair analysis of images from a range of different specimens in single-particle electron cryomicroscopy. J Mol Biol **413**:1028–1046

Heuser JE (2011) The origins and evolution of freeze-etch electron microscopy. J Electron Microsc **60**:S3–S29

Hooley P, Whitehead MP, Brown MRW (2008) Eukaryote polyphosphate kinases: is the 'Kornberg' complex ubiquitous? Trends Biochem Sci **33**:577–582

Hong-Hermesdorf A, Miethke M, Gallaher SD, Kropat J, Dodani SC, Chan J, Barupala D, Domaille DW, Shirasaki DI, Loo JA, Weber PK, Pett-Ridge J, Stemmler TL, Chang CJ, Merchant SS (2014) Subcellular metal imaging identifies dynamic sites of Cu accumulation in *Chlamydomonas*. Nature Chem Biol **10**:1034–1042

Hothorn M, Neumann H, Lenherr ED, Wehner M, Rybin V, Hassa PO, Uttenweiler A, Reinhardt M, Schmidt A, Seiler J, Ladurner AG, Hermann C, Scheffzek K, Mayer A (2009) Catalytic core of a membrane-associated eukaryotic polyphosphate polymerase. Science **324**:513–515

Hsu S-H, Hsiao Y-Y, Liu P-F, Lin S-M, Luo Y-Y, Pan R-L (2009) Purification, characterization, and spectral analyses of histidine-tagged vacuolar H+-pyrophosphatase expressed in yeast. Bot Stud **50**:291–301

Huang G, Bartlett PJ, Thomas AP, Moreno SNJ, Docampo R (2013) Acidocalcisomes of *Trypanosoma brucei* have an inositol 1,4,5-triphosphate receptor that is required for growth and infectivity. Proc Natl Acad Sci USA **110**:1887–1892

Huang G, Fang J, Sant'Anna C, Li Z-H, Wellems DL, Rohloff P, Docampo R (2011) Adaptor protein-3 (AP-3) complex mediates the biogenesis of acidocalcisomes and is essential for growth and virulence of *Trypanosoma brucei*. J Biol Chem **286**:36619–36630

Huang G, Ulrich PN, Storey M, Johnson D, Tischer J, Tovar JA, Moreno SNJ, Orlando R, Docampo R (2014) Proteomic analysis of the acidocalcisome, an organelle conserved from bacteria to human cells. PLoS Pathog **10**:e1004555

Huizing M, Helip-Wooley A, Westbroek W, Gunay-Aygun M, Gahl WA (2008) Disorders of lysosome-related organelle biogenesis: clinical and molecular genetics. Annu Rev Genom Human Genet **9**:359–386

Kaneko Y, Nitta K, Nagayama K (2007) Observation of *in vivo* DNA in ice embedded whole cyanobacterial cells by Hilbert differential contrast transmission electron microscopy (HDC-TEM). Plasma Fusion Res **2**:S1007

Karlson B, Potter D, Kuylenstierna M, Andersen RA (1996) Ultrastructure, pigment composition, and 18S rRNA gene sequence for *Nannochloropsis granulata* sp. nov (Monodopsidaceae, Eustigmatophyceae), a marine ultraplankter isolated from the Skagerrak, northeast Atlantic Ocean. Phycologia **35**:253–260

Kaska DD, Piscopo IC, Gibor A (1985) Intracellular calcium redistribution during mating in *Chlamydomonas reinhardii*. Exp Cell Res **160**:371–379

Kellosalo J, Kajander T, Palmgren MG, Lopez-Marques RL, Goldman A (2007) Heterologous expression and purification of membrane-bound pyrophosphatases. Protein Express Purif **79**:25–34

Kim EJ, Zhen R-G, Rea PA (1994) Heterologous expression of plant vacuolar pyrophosphatase in yeast demonstrates sufficiency of the substrate-binding subunit for proton transport. Proc Natl Acad Sci USA **91**:6128–6132

Klein U, Chen C, Gibbs M, Platt-Aloia KA (1983) Cellular fractionation of *Chlamydomonas reinhardii* with emphasis on the isolation of the chloroplast. Plant Physiol **72**:481–487

Klompmaker SH, Kohl K, Fasel N, Mayer A (2017) Magnesium uptake by connecting fluid-phase endocytosis to an intracellular inorganic cation filter. Nat Commun **18**:1879

Kobayashi Y, Ohnuma M, Kuroiwa T, Tanaka K, Hanaoka M (2010) The basics of cultivation and molecular genetic analysis of unicellular red alga *Cyanidioschyzon merolae*. J. Endocytosis Cell Res **20**:53–61

Kohl K, Zangger H, Rossi M, Isorce N, Lye L-F, Owens KL, Beverley SM, Mayer A, Fasel N (2018) Importance of polyphosphate in the *Leishmania* life cycle. Microb Cell **5**:371–384

Komine Y, Eggink LL, Park H, Hoober JK (2000) Vacuolar granules in *Chlamydomonas reinhardtii*: polyphosphate and a 70-kDa polypeptide as major components. Planta **210**:897–905

Komine Y, Park H, Wolfe GR, Hoober JK (1996) Secretory granules in the cytoplasm of a wall-less mutant of *Chlamydomonas reinhardtii* contain processed light-harvesting complex apoproteins and HSP70. J Photochem Photobiol B: Biol **36**:301–306

Kornberg A, Rao NN, Ault-Riché D (1999) Inorganic polyphosphate: a molecule of many functions. Annu Rev Biochem **68**:89–125

Lander N, Chiurillo MA, Storey M, Vercesi AE, Docampo R (2016) CRISPR/Cas9-mediated endogenous C-terminal tagging of *Trypanosoma cruzi* genes reveals the acidocalcisome localization of the inositol 1,4,5-triphosphate receptor. J Biol Chem **291**:25505–25515

Lee N, Gannavaram S, Selvapandiyan A, Debrabant A (2007) Characterization of metacaspases with trypsin-like activity and their putative role in programmed cell death in the protozoan parasite *Leishmania*. Eukaryot Cell **6**:1745–1757

Lewin RA (1952) Ultraviolet induced mutations in *Chlamydomonas moewusii* Gerloff. J Gen Microbiol **6**:233–248

Li F-J, He CY (2014) Acidocalcisome is required for autophagy in *Trypanosoma brucei*. Autophagy **10**:1978–1988

Luo A, Qiao H, Zhang Y, Shi W, Ho SY, Xu W, Zhang A, Zhu C (2010) Performance of criteria for selecting evolutionary models in phylogenetics: a comprehensive study based on simulated datasets. BMC Evol Biol **10**:242

Luo S, Ruiz FA, Moreno SNJ (2005) The acidocalcisome Ca^{2+}-ATPase (TgA1) of *Toxoplasma gondii* is required for polyphosphate storage, intracellular calcium homeostasis and virulence. Mol Microbiol **55**:1034–1045

Luoto HH, Belogurov GA, Baykov AA, Lahti R, Malinen AM (2011) Na^+-Translocating membrane pyrophosphatases are widespread in the microbial world and evolutionarily precede H^+-translocating pyrophosphatases. J Biol Chem **286**:21633–21642

Marchesini N, Ruiz FA, Vieira M, Docampo R (2002) Acidocalcisomes are functionally linked to the contractile vacuole of *Dictyostelium discoideum*. J Biol Chem **277**:8146–8153

Martin NC, Goodenough UW (1975) Gametic differentiation in *Chlamydomonas reinhardtii* I. Production of gametes and their fine structure. J Cell Biol **67**:587–605

Martin P, Dyhrman ST, Lomas MW, Poulton NJ, Van Mooy BAS (2014) Accumulation and enhanced cycling of polyphosphate by Sargasso Sea plankton in response to low phosphorus. Proc Natl Acad Sci USA **111**:8089–8094

Martinez J, Truffault V, Hothorn M (2015) Structural determinants for substrate binding and catalysis in triphosphate tunnel metalloenzymes. J Biol Chem **290**:23348–23360

Martinez R, Wang Y, Benaim G, Benchimol M, de Souza W, Scott DA, Docampo R (2002) A proton pumping pyrophosphatase in the Golgi apparatus and plasma membrane vesicles of *Trypanosoma cruzi*. Mol Biochem Parasitol **120**:205–213

McIntosh MT, Vaidya AB (2002) Vacuolar type H+ pumping pyrophosphatases of parasitic protozoa. Int J Parasitol **32**: 1–14

Medeiros LCS, Gomes F, Maciel LRM, Seabra SH, Docampo R, Moreno S, Plattner H, Hentschel J, Kawazoe U, Barrabin H, De Souza W, Damatta RA, Miranda K (2011) Volutin granules of *Eimeria* parasites are acidic compartments and have physiological and structural characteristics similar to acidocalcisomes. J Eukaryot Microbiol **58**:416–423

Minh BQ, Nguyen MAT, Haeseler von A (2013) Ultrafast approximation for phylogenetic bootstrap. Mol Biol Evol **30**:1188–1195

Miranda K, de Souza W, Plattner H, Hentschel J, Kawazoe U, Fang J, Moreno SNJ (2008) Acidocalcisomes in apicomplexans parasites. Exp Parasitol **118**:2–9

Miranda K, Pace DA, Cintron R, Rodrigues JCF, Fang J, Smith A, Rohloff P, Coelho E, de Haas F, deSouza W, Coppens I, Sibley LD, Moreno SNJ (2010) Characterization of a novel organelle in *Toxoplasma gondii* with similar composition and function to the plant vacuole. Mol Microbiol **76**:1358–1375

Montalvetti A, Rohloff P, Docampo R (2004) A functional aquaporin co-localizes with the vacuolar proton pyrophosphatase to acidocalcisomes and the contractile vacuole complex of *Trypanosoma cruzi*. J Biol Chem **279**:38673–38682

Moreno B, Rodrigues CO, Bailey BN, Urbine JA, Moreno SNJ, Docampo R, Oldfield E (2002) Magic-angle spinning ^{31}P NMR spectroscopy of condensed phosphates in parasitic protozoa: visualizing the invisible. FEBS Lett **523**:207–212

Moreno SNJ, Docampo R (2009) The role of acidocalcisomes in parasitic protists. J Eukaryot Microbiol **56**:208–213

Moreno SNJ, Docampo R (2013) Polyphosphate and its diverse functions in host cells and pathogens. PLoS Pathog **9**, e1003230

Moreno-Sanchez D, Hernandez-Ruiz L, Ruiz FA, Docampo R (2012) Polyphosphate is a novel pro-inflammatory regulator of mast cells and is located in acidocalcisomes. J Biol Chem **287**:28435–28444

Morrissey JH, Choi SH, Smith SA (2012) Polyphosphate: an ancient molecule that links platelets, coagulation and inflammation. Blood **119**:5972–5979

Muller F, Mutch NJ, Schenk WA, Smith SA, Esterl L, Spronk HM, Schmidbauer S, Gahl WA, Morrissey JH, Renne T (2009) Platelet polyphosphates are proinflammatory and procoagulant mediators in vivo. Cell **139**:1–14

Nagasaka S, Nishizawa NK, Watanabe T, Mori S, Yoshimura E (2003) Evidence that electron-dense bodies in *Cyanidium caldarium* have an iron-storage role. BioMetals **16**:465–470

Nikolić JD, Živaanović VD, Matijaševic D, Stojanović JN, Snežana R, Grujić SR, Smiljanić SV, Topalović VS (2016) Crystallization and sintering behaviors of the polyphosphate glass doped with Zn and Mn. J Term Anal Calorim **124**:585–592

Niyogi S, Jimenez V, Girard-Dias W, de Souza W, Miranda K, Docampo R (2015) Rab32 is essential for maintaining functional acidocalcisomes, and for growth and infectivity of *Trypanosoma cruzi*. J Cell Sci **128**:2363–2373

Omelon SJ, Grynpas MD (2008) Relationships between polyphosphate chemistry, biochemistry, and biomineralization. Chem Rev **108**:4694–4715

Penen JM, Isaurea M-P, Dobritzsch D, Bertalanc I, Gontier E, Le Coustumer P, Schaumlöffel D (2016) Chemical bioimaging for the subcellular localization of trace elements by high contrast TEM, TEM/X-EDS, and NanoSIMS. J Trace Elem Med Biol **37**:62–68

Penen F, Isaure MP, Dobritzsch D, Bertalan I, Castillo-Michel H, Proux O, Gontier E, LeCoustumer P, Schaumlöffel D (2017) Pools of cadmium in *Chlamydomonas reinhardtii* revealed by chemical imaging and XAS spectroscopy. Metallomics **9**:910–923

Perez-Castineira JR, Alvar J, Ruiz-Perez LM, Serrano A (2002) Evidence for a wide occurrence of proton-translocating pyrophosphatase genes in parasitic and free-living protozoa. Biochem Biophys Res Comm **294**:567–573

Pérez-Pérez ME, Couso I, Crespo JL (2012) Carotenoid deficiency triggers autophagy in the model green alga *Chlamydomonas reinhardtii*. Autophagy **8**:376–388

Pick U, Weiss M (1991) Polyphosphate hydrolysis within acidic vacuoles in response to amine-induced alkaline stress in the halotolerant alga *Dunaliella salina*. Plant Physiol **97**: 1234–1240

Pinto-Martinez AK, Rodriquez-Duràn J, Serrano-Martin X, Hernandez-Rodriquez V, Benalm G (2018) Mechanism of action of miltefosine on *Leishmania donovani* involves the impairment of acidocalcisome function and the activation of the sphingosine-dependent plasma membrane Ca^{2+} channel. Antimicrob Agents Chemother **62**:e01614–17

Rao NN, Gomez-Garcia MR, Kornberg A (2009) Inorganic polyphosphate essential for growth and survival. Annu Rev Biochem **78**:605–647

Ramakrishnan S, Docampo R (2018) Membrane proteins in trypanosomatids involved in Ca^{2+} homeostasis and signaling. Genes **9**:304

Ramakrishnan S, Asady B, Docampo R (2018) Acidocalcisome-mitochondrion membrane contact sites in *Trypanosoma brucei* (2018). Pathogens **7**:33

Ramundo S, Casero D, Mühlhaus T, Hemme D, Sommer F, Crèvecoeur M, Rahire M, Schroda M, Rusch J, Goodenough U, Pellegrini M, Pérez-Pérez ME, Crespo JL, Schaad O, Civic N, Rochaix JD (2014) Conditional depletion of the *Chlamydomonas* chloroplast ClpP protease activates nuclear genes involved in autophagy and plastid protein quality control. Plant Cell **26**:2201–2222

Raposo G, Marks MS, Cutler DF (2007) Lysosome-related organelles: driving post-Golgi compartments into specialization. Curr Opin Cell Biol **19**:394–401

Rea PA, Kim Y, Sarafian V, Poole RJ, Davies JM, Sanders D (1992) Vacuolar H^+-translocating pyrophosphatases: a new category of ion translocase. Trends Biochem Sci **17**: 348–353

Robinson DG, Hoppenrath M, Oberback K, Luykx P, Ratajczak R (1998) Localization of pyrophosphatase and V-ATPase in *Chlamydomonas reinhardtii*. Bot Acta **111**:108–122

Rodrigues CO, Scott DA, Docampo R (1999) Characterization of a vacuolar pyrophosphatase in *Trypanosoma brucei* and its localization to acidocalcisomes. Mol Cell Biol **19**: 7712–7723

Rohloff P, Montalvetti A, Docampo R (2004) Acidocalcisomes and the contractile vacuole complex are involved in osmoregulation in *Trypanosoma cruzi*. J Biol Chem **279**:52270–52281

Ruiz FA, Marchesini N, Seufferhald M, Govindjee, Docampo R (2001a) The polyphosphate bodies of *Chlamydomonas reinhardtii* possess a proton-pumping pyrophosphatase and are similar to acidocalcisomes. J Biol Chem **276**: 46196–46203

Ruiz FA, Rodrigues CO, Docampo R (2001b) Rapid changes in polyphosphate content within acidocalcisomes in response to cell growth, differentiation, and environmental stress in *Trypanosoma cruzi*. J Biol Chem **276**:26114–26121

Ruiz FA, Luo S, Moreno SNJ, Docampo R (2004a) Polyphosphate content and fine structure of acidocalcisomes of *Plasmodium falciparum*. Microsc Microanal **10**:563–567

Ruiz FA, Lea CR, Oldfield E, Docampo R (2004b) Human platelet dense granules contain polyphosphate and are similar to acidocalcisomes of bacteria and unicellular eukaryotes. J Biol Chem **279**:44250–44257

Salisbury JL (1982) Calcium-sequestering vesicles and contractile flagellar roots. J Cell Sci **58**:433–443

Schilling RK, Tester M, Marschner P, Plett DC, Roy SJ (2017) AVP1: one protein, many roles. Trends Plant Sci **22**:154–162

Schmollinger S, Mühlaus T, Boyle NR, Blaby IK, Casero D, Mettler T, Moseley JL, Kropat J, Sommer F, Strenkert D, Hemme D, Pellegrini M, Grossman AR, Stitt M, Schroda M, Merchant SS (2014) Nitrogen-sparing mechanisms in *Chlamydomonas* affect the transcriptome, the proteome, and photosynthetic metabolism. Plant Cell **26**:1410–1435

Scott DA, Docampo R, Dvorak JA, Shi S, Leapman RD (1997) In situ compositional analysis of acidocalcisomes in *Trypanosoma cruzi*. J Biol Chem **272**:28020–28029

Scott DA, Docampo R (2000) Characterization of isolated acidocalcisomes of *Trypanosoma cruzi*. J Biol Chem **275**:24215–24221

Segami S, Asaoka M, Kinoshita S, Fukuda M, Nakanishi Y, Mawshima M (2017) Biochemical, structural and physiological characteristics of vacuolar H^+-pyrophosphatase. Plant Cell Physiol **59**:1300–1308

Serrano A, Perez-Castineira JR, Baltscheffsky M, Baltscheffsky H (2007) H+-PPases: yesterday, today and tomorrow. Life **59**:76–83

Seufferheld M, Lea CR, Vieira M, Oldenfield E, Docampo R (2004) The H^+-pyrophosphatase of *Rhodospirillum rubrum* is predominantly located in polyphosphate-rich acidocalcisomes. J Biol Chem **279**:61193–61202

Seufferheld M, Vieira MCF, Ruiz FA, Rodrigues CO, Moreno SNJ, Docampo R (2003) Identification of organelles in bacteria similar to acidocalcisomes of unicellular eukaryotes. J Biol Chem **278**:29971–29978

Seufferheld MJ, Kim KM, Whitfield J, Valerio A, Caetano-Anollés G (2011) Evolution of vacuolar proton pyrophosphatase domains and volutin granules: clues into the early evolutionary origin of the acidocalcisome. Biol Direct **6**:50

Severs NJ (2007) Freeze-fracture electron microscopy. Nature Protocols **2**:547–576

Shah NR, Wilkinson C, Harborne SPD, Turku A, Li K-M, Sun Y-J, Harris S, Goldman A (2017) Insights into the mechanism of membrane pyrophosphatases by combining experiment and computer simulation. Struct Dynam **4**:032105

Shebanova A, Ismagulova T, Solovchenko A, Baulina O, Lovakova E, Ivanova A, Moiseenko A, Shaitan K, Polshakov V, Nedbal L, Gorelova O (2017) Versatility of the green microalga cell vacuole function as revealed by analytical transmission electron microscopy. Protoplasma **254**:1323–1340

Siderius M, Musgrave A, van den Ende H, Koerten H, Cambier P, van der Meer P (1996) *Chlamydomonas eugametos* (Chlorophyta) stores phosphate in polyphosphate bodies together with calcium. J Phycol **32**:402–409

Steinmann ME, Schmidt RS, Bütikofer P, Mäser P, Sigel E (2017) TblRK is a signature sequence free potassium channel from *Trypanosoma brucei* locating to acidocalcisomes. Sci Rep **7**:656

Sueoka N (1960) Mitotic replication of deoxyribonucleic acid in *Chlamydomonas reinhardi*. Proc Natl Acad Sci USA **46**:83–91

Tommi K, Juho K, Adrian G (2013) Inorganic pyrophosphatases: one substrate, three mechanisms. FEBS Lett **587**:1863–1869

Tsai J-Y, Kellosalo J, Sun Y-J, Goldman A (2014) Proton/sodium pumping pyrophosphatases: the last of the primary ion pumps. Curr Opin Struct Biol **27**:38–47

Ulrich PN, Lander N, Kurup SP, Reiss L, Brewer J, Medeiros LCS, Miranda K, Docampo R (2014) The acidocalcisome vacuolar transporter chaperone 4 catalyzes the synthesis of polyphosphate in insect-stages of *Trypanosoma brucei* and *T. cruzi*. J Eukaryot Microbiol **61**:155–165

Vannier-Santos MA, Martiny A, Lins U, Urbina JA, Borges VA, de Souza W (1999) Impairment of sterol bioshythesis leads to phosphorus and calcium accumulation in *Leishmania* acidocalcisomes. Microbiology **145**:3213–3220

Venter M, Groenewald J-H, Botha FC (2006) Sequence analysis and transcriptional profiling of two vacuolar H+-pyrophosphatase isoforms in *Vivis vinifera*. J Plant Res **119**:469–478

Vercesi AE, Moreno SNJ, Docampo R (1994) Ca^{2+}/H^+ exchange in acidic vacuoles of *Trypanosoma brucei*. Biochem J **304**:227–233

Weiss TL, Roth R, Goodson C, Vitha S, Black I, Azadi P, Rusch J, Holzenburg A, Devarenne TP, Goodenough U (2012) Colony organization in the green alga *Botryococcus braunii* (Race B) is specified by a complex extracellular matrix. Eukaryot Cell **11**:1424–1440

Wild R, Gerasimaite R, Jung J-Y, Truffault V, Pavlovic I, Schmidt A, Saiardi A, Jessen HJ, Poirier Y, Hothorm M, Mayer A (2016) Control of eukaryotic phosphate homeostasis by inositol polyphosphate sensor domains. Science **352**:986–990

Yagisawa F, Nishida K, Kuroiwa H, Nagata T, Kuroiwa T (2007) Identification and mitotic partitioning strategies of vac-

uoles in the unicellular red alga *Cyanidioschyzon merolae*. Planta **226**:1017–1029

Yagisawa F, Nishida K, Yoshida M, Ohnuma M, Shimada T, Fujiwara T, Yoshida Y, Misumi O, Kuroiwa H, Kuroiwa T (2009) Identification of novel proteins in isolated polyphosphate vacuoles in the primitive red alga *Cyanidioschyzon merolae*. Plant J **60**:882–893

Zaremba-Niedzwiedzka K, Caceres EF, Saw JH, Bäckström D, Juzokaite L, Vancaester E, Seitz KW, Anantharaman K, Starnawski P, Kjeldsen KU, Stott MB, Nunoura T, Banfield JF, Schramm A, Baker BJ, SpangA. Ettema TJG (2017) Asgard archaea illuminate the origin of eukaryotic cellular complexity. Nature **541**:353–358

Available online at www.sciencedirect.com

ScienceDirect